Rea, D.K., Basov, I.A., Scholl, D.W., and Allan, J.F. (Eds.), 1995
Proceedings of the Ocean Drilling Program, Scientific Results, Vol. 145

37. BIOSTRATIGRAPHIC AND MAGNETOSTRATIGRAPHIC SUMMARY[1]

John A. Barron,[2] Ivan A. Basov,[3] Luc Beaufort,[4] Gilles Dubuisson,[5] Andrey Y. Gladenkov,[3] Joseph J. Morley,[6] Makoto Okada,[7] Gunnar Ólafsson,[8] Dorothy K. Pak,[9] Andrew P. Roberts,[10] Valery V. Shilov,[11] and Robin J. Weeks[12]

ABSTRACT

The magnetostratigraphic and biostratigraphic results of Ocean Drilling Program Sites 881–884 and 887 are summarized and combined to form age vs. depth models for these sites. The recovery of continuous magnetostratigraphic records of the upper lower Miocene through Pleistocene section at Sites 884 and 887 allows the first direct calibration of diatom and radiolarian datum levels with magnetostratigraphy between magnetic Subchrons C5En and C3Bn (18.317–6.744 Ma) in the North Pacific. Based on these records and temporally shorter magnetostratigraphic records at Sites 881–883, at least 25 diatom and 22 radiolarian datum levels appear to be isochronous in the late early Miocene through Pleistocene of the North Pacific. The use of calcareous nannofossils for biostratigraphy of the post-early middle Miocene appears to be limited to the late Pliocene and Quaternary in sections sampled by Leg 145.

Biostratigraphy indicates that a composite section of Sites 883 and 884 represents a relatively complete record of the lower Eocene through the lower Miocene, although carbonate preservation is best and the section is less complicated by reworking at Site 883. Primary biostratigraphic control is provided by calcareous nannofossils. A large part of the upper middle Eocene and upper Eocene is missing at hiatuses at both Sites 883 and 884.

A condensed upper Paleocene section is present at Site 883, unconformably overlying uppermost Cretaceous sediments. Late Maestrichtian calcareous nannofossils are documented in Site 883 immediately above the basalt.

INTRODUCTION

Ocean Drilling Program (ODP) Leg 145 cored 25 holes at seven sites in a west to east transect of the subarctic North Pacific (Fig. 1). Three of these sites (882, 883, and 887) that were cored on top of seamounts, where carbonate-bearing sediments were relatively free of terrigenous debris, offered the best possibility of high-resolution paleoceanographic studies. Site 884, on the east flank of the Detroit Seamount, was cored in order to obtain a comparative record of deep-sea sedimentation and to record the history of the Meiji sediment tongue. Site 881 was selected to be a northern extension of the south-to-north paleoceanographic transect which began off Japan on Deep Sea Drilling Project (DSDP) Leg 86, whereas Sites 885 and 886 were located in the low-biologic-productivity region of the central North Pacific, where a good record of eolian deposition was expected (Rea, Basov, Janecek, Palmer-Julson, et al., 1993).

The main purpose of this paper is to present age vs. depth models for Sites 881–884 and 887 based on papers in this volume dealing with magnetostratigraphy (Weeks et al.; Dubuisson et al.) and biostratigraphy (Barron and Gladenkov; Basov; Beaufort and Ólafsson; Gladenkov and Barron; Morley and Nigrini; Ólafsson and Beaufort; Pak and Miller; Shilov). High-resolution chronology for the Pleistocene and Pliocene is not treated here, and the reader is referred to the orbital time scale developed by Tiedemann and Haug (this volume) for Site 882 and oxygen isotope studies by Keigwin (this volume) for Site 883, as well as radiolarian studies by Morley et al. (this volume) for Sites 881, 883, and 887. In general, the biostratigraphic zonation of the individual sites is not discussed because only the diatom zonation (Barron and Gladenkov, this volume) is widely accepted and widely applicable in the North Pacific. Similarly, age vs. depth models for Sites 885 and 886 are not treated here because they are thoroughly presented by Dickens et al. (this volume) and Snoeckx et al. (this volume).

METHODS

Time Scale/Chronological Framework

Leg 145 studies employs the Cande and Kent (1992) geomagnetic-polarity time scale, and the ages for biostratigraphic datums, which were previously calibrated to the Berggren et al. (1985a, 1985b) time scale, are updated accordingly. This recalculation involves reinterpolation of the age of a particular datum level within a given magnetic subchron using the Cande and Kent (1992) ages for the onset and termination of that subchron. The correlation of the geologic epochs and periods used follows that of Berggren et al. (1985a, 1985b) with the exception of the Miocene/Pliocene boundary, where the calibration of Zijderveld et al. (1986) was used. Whenever possible, ages are assigned to sediments based on magnetostratigraphy. Other sediments are dated by employing previously published calibration of biostrati-

[1] Rea, D.K., Basov, I.A., Scholl, D.W., and Allan, J.F. (Eds.), 1995. *Proc. ODP, Sci. Results*, 145: College Station, TX (Ocean Drilling Program).

[2] U.S. Geological Survey, MS 915, Menlo Park, CA 94025, U.S.A.
[3] Institute of the Lithosphere, Russian Academy of Sciences, Staromonetny per. 22, Moscow 109180, Russia.
[4] Laboratoire de Géologie du Quaternaire, CNRS Luminy, case 907, 13288 Marseille cedex 09, France.
[5] Laboratoire de Géologie, Ecole Normale Supérieure, 24 rue Lhomond, 75231 Paris cedex 05, France.
[6] 32 West End Ave., Westwood, NJ 07675, U.S.A.
[7] Ocean Research Institute, University of Tokyo 1-15-1 Minamidai, Nakano-ku, Tokyo 164, Japan.
[8] Marine Research Institute, Hafrannsoknarstofnunin, Skulagata 4, P.O. Box 1390, IS-121, Reykjavik, Iceland.
[9] Lamont-Doherty Earth Observatory, Palisades, NY 10964, U.S.A.
[10] Department of Geology, University of California, Davis, CA 95616, U.S.A.
[11] Institute of Geology and Mineral Resources of the Oceans, Maklina Ave. 1, St. Petersburg 109121, Russia.
[12] Department of Geological Sciences, University of Washington, Seattle, WA 98195, U.S.A.

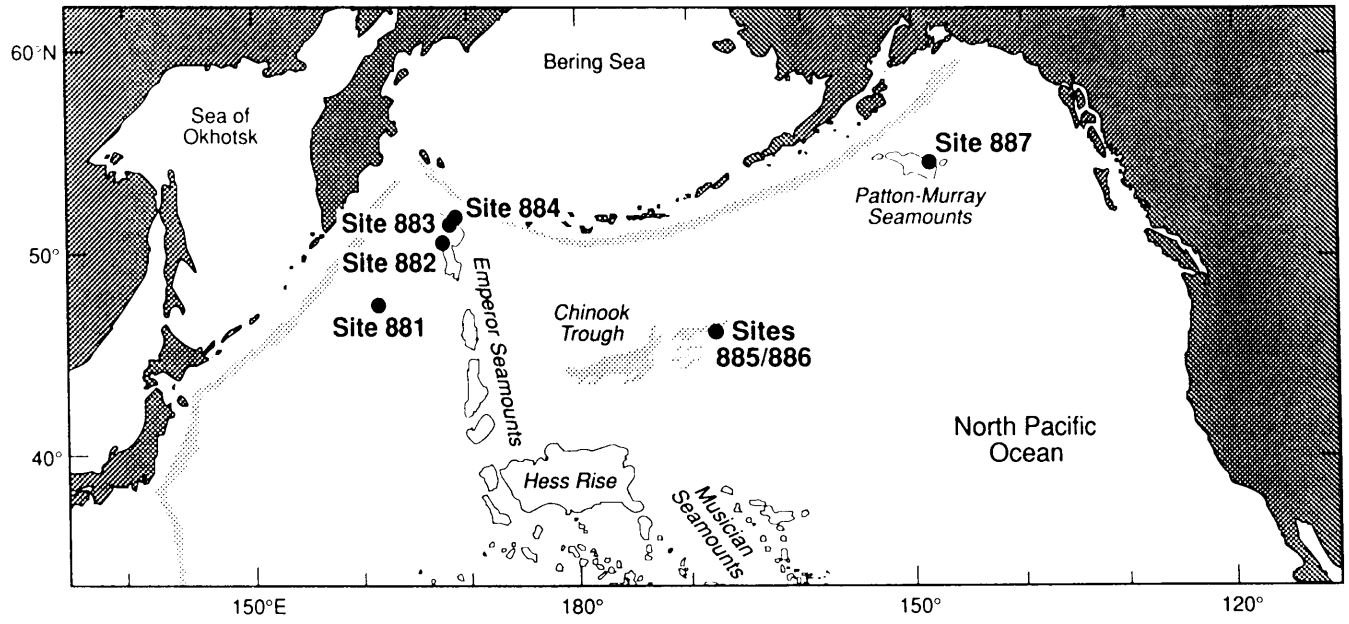

Figure 1. Location of sites cored in the North Pacific.

graphic datum levels to magnetostratigraphy in the North Pacific and elsewhere (see individual chapters).

In most cases, ages listed in the tables of this chapter come directly from the individual chapters and are those that the individual authors believe to be most reliable. However, the ages of Pak and Miller (this volume) were updated to correspond with the Cande and Kent (1992) time scale because they were referenced to the Berggren et al. (1985a) time scale. In addition, selected Paleogene planktonic foraminiferal datum levels recorded by Basov (this volume) were assigned ages according to Berggren et al. (1985a) and Aubry et al. (1988) and then updated to the Cande and Kent (1992) time scale.

RESULTS

Site 881

An apparently continuous sequence of upper Miocene through Quaternary sediments was recovered at Site 881 (47°6.1′N, 161°29.5′E; 5531 m water depth). The 364-m-thick section consists of diatom ooze overlain by clayey diatom ooze, the latter containing numerous ash layers. Diatoms and radiolarians generally are common to abundant and moderately well to well preserved throughout the section recovered at Site 881, whereas calcareous nannofossils and foraminifers occur at only a few intervals and at very low abundances in sediments from the four holes drilled at this site.

The magnetostratigraphy at Site 881 extends down to the uppermost part of the Gilbert Reversed-Polarity Chron (Shipboard Scientific Party, 1993a; Weeks et al., this volume). Table 1 gives the estimated ages of paleomagnetic polarity boundaries and microfossil datum levels recorded in Holes 881B, 881C, and 881D, the interval over which they occur, and the depth of this interval in meters below sea floor (mbsf).

An age vs. depth curve for Site 881 is shown in Figure 2 using paleomagnetic polarity boundaries (above 210 mbsf) and diatom and radiolarian datum levels (Table 1) that have previously been calibrated to magnetostratigraphy. At about 165 mbsf the sediment accumulation rate decreases abruptly down section from 100 m/m.y. to 33 m/m.y., coinciding with an abrupt change in lithology from clayey diatom ooze rich in ashes above to diatom ooze below (Shipboard Scientific Party, 1993a). The change in physical and magnetic properties at this level is likewise abrupt (Shipboard Scientific Party, 1993a), and seismic stratigraphy recognizes a region-wide reflector at this horizon (Hamilton, this volume).

Unconformities

An unconformity is suggested by the age vs. depth curve (Fig. 2) at about 270 mbsf, where the latest Miocene interval, corresponding to about 6.1 to 5.3 Ma, may be missing. A widespread reflector is evident at this depth from seismic reflection data (Hamilton, this volume); however, no lithologic change or major change in the natural gamma ray or other logs is apparent at this depth (Shipboard Scientific Party, 1993a).

A second possible unconformity is inferred at about 325 mbsf in the unrecovered interval between Cores 881C-35X and 881C-36X, based on the coincidence of diatom and radiolarian datum levels that range in age from ca. 7.7 to 7.1 Ma (Table 1; Fig. 2). Abrupt downhole increase in the weight-percent of potassium, thorium, and uranium are indicated by the natural gamma-ray log, and the Gamma-ray attenuation porosity evaluator (GRAPE) recorded an abrupt increase in bulk density at this depth (Shipboard Scientific Party, 1993a).

Site 882

An apparently continuous sequence of upper Miocene through Quaternary sediments was recovered at Site 882 on the top of the Detroit Seamount at 50°21.8′N; 167°36.0′E (3255 m water depth). The two holes that were drilled penetrated a 398-m-thick section consisting of diatom ooze with intervals of clayey diatom ooze and minor carbonate materials.

Moderately well-preserved calcareous nannofossils occur in abundances ranging from rare to abundant but with little diversity among species, down to approximately 227 mbsf, where they become rare. Moderately well-preserved calcareous foraminifers are present

Table 1. Age, interval, and depth of magnetostratigraphic polarity boundaries and biostratigraphic datum levels in Holes 881B, 881C, and 881D.

		Datum	Age (Ma)	Core, section, interval (cm) 145-881B-	Depth (mbsf)	Core, section, interval (cm) 145-881C-	Depth (mbsf)
R1	LO	*Lychnocanoma nipponica sakaii*	0.05	Above 1H-CC	/5.5	1H-1, 21–22/1H-CC	0.2/3.8
D1	LO	*Simonseniella curvirostris*	0.30	3H-CC/4H-CC	24.5/34.0	3H-CC/4H-CC, 2	2.8/32.3
R2	LO	*Stylacontarium acquilonium*	0.40	2H-CC/3H-CC	15.0/24.5	3H-CC/4H-CC, 2	2.8/32.3
R3	LO	*Stylatractus universus*	0.55	2H-CC/3H-CC	15.0/24.5	3H-CC/4H-CC, 2	2.8/32.3
R4	LO	*Anthocyrtella (?) callopsma*	0.62			4H-CC/5H-CC	32.3/41.8
	B	C1n.1n	0.78	6H-3, 0	46.50	6H-5, 30	48.1
R5	LO	*Lamprocyrtis neoheteroporos*	0.85	7H-CC/8H-CC	62.5/72.0	5H-CC/6H-CC	41.8/51.3
	T	C1r.1n	0.984	7H-2, 55	55.05	7H-5, 30	57.6
D2	LO	*Rhizosolenia matuyamai*	0.91–1.04			7H-CC/8H-CC	60.8/70.3
R6	LO	*Eucyrtidium matuyamai*	1.00	7H-CC/8H-CC	62.5/72.0	6H-CC/7H-CC	51.3/60.8
	B	C1r.1r	1.049	7H-6, 120	61.70	8H-2, 20 or 8H-4, 140	62.5 or 66.7
D3	FO	*Rhizosolenia matuyamai*	0.98–1.12			8H-CC/9H-CC	70.3/79.8
D4	LCO	*Actinocyclus oculatus*	1.0	7H-CC/8H-CC	62.5/72.0	7H-CC/8H-CC	60.8/70.3
R7	LO	*Sphaeropyle robusta*	1.5–1.7			10H-CC/11H-CC	89.3/98.8
D5	FO	*Simonseniella curvirostris*	1.58	10H-CC/11H-CC	91.0/100.5	11H-CC/12H-CC	98.8/108.3
	T	C2n.1n	1.757	12H-3, 10	103.60	12H-5, 20?	105?
	B	C2n.1n	1.983	12H-6, 95	108.95	13H-2, 10?	109.9?
D6	LO	*Neodenticula koizumii*	2.0	11H-CC/12H-CC	100.5/110.0	11H-CC/12H-CC	98.9/108.3
R8	FO	*Eucyrtidium matuyamai*	2.0	12H-CC/13H-CC	110.0/119.5	13H-CC/14H-CC	117.8/127.3
	T	C2n.2n	2.197	13H-6, 30	117.8/119.8	14H-4, 75	123.05
	B	C2n.2n	2.229	14H-2, 50?	121.5?	14H-7, 70	127.50
D7	LO	*Thalassiosira convexa*	2.4	15H-CC/16H-CC?	138.5/148.0		
	T	"X" anomaly	2.42	16H-1, 0	138.50	16H-2, 120	139.50
	B	"X" anomaly	2.441	16H-4, 70	143.70	16H-6, 10	144.40
	T	C2An.1n	2.6	18H-5, 130	164.80		
				145-881D-			
	T	C2An.1n	2.6	1H-6, 5/2H-1, 0	163.0/164.5		
D8	LCO	*Neodenticula kamtschatica*	2.63–2.7	1H-CC/2H-CC	164.75/174.0	18X-CC/21H-1, 25	162.3/182.0
D9	FO	*Neodenticula seminae*	2.7	1H-CC/2H-CC	164.75/174.0	18X-CC/21H-1, 25	162.3/182.0
R9	FO	*Cycladophora davisiana davisiana*	2.90	2H-CC/3H-CC	174.0/183.5	18X-CC/21H-CC	162.3/191.2
	B	C2An.1n	3.054	3H-3, 120	178.2		
	T	C2An.2n	3.127	3H-5, 150	181.5		
D10	LO	*Thalassiosira marujamica*	3.1–3.2	3H-5, 125/3H-CC	181.25/183.5	18X-CC/21H-1, 25	162.3/182.0
	B	C2An.2n	3.221	4H-1, 70	184.2		
	T	C2An.3n	3.325	4H-2, 120	186.2		
	B	C2An.3n	3.553	5H-4, 40/5H-6, 100	197.9/201.5		
	T	C3n.1n	4.033	6H-6, 80	210.8		
D11	FO	*Neodenticula koizumii*	3.51–3.85	Below 6H-CC	Below 212.0		
D12	FO	*Actinocyclus oculatus*	3.65–3.85	Below 6H-CC	Below 212.0	23X-CC/25X-CC	209.7/228.7
R10	LO	*Dictyophimus bullatus*	4.2	Below 6H-CC	Below 212.0	23X-CC/25X-1, 20–21	209.7/219.2
D13	LO	*Thalassiosira jacksonii* (plicate)	4.5–4.6			23X-CC/25X-CC	209.7/228.7
D14	FO	*Thalassiosira latimarginata*	4.8–4.9			27X-CC/29X-CC	248.0/267.2
D15	FO	*Thalassiosira oestrupii*	5.3			29X-CC/30X-CC	267.2/276.9
R11	FO	*Dictyophimus bullatus*	5.60			27X-5, 20–21/29X-1, 20–21	244.5/257.8
D16	LCO	*Rouxia californica*	6.3			30X-CC/32X-1, 46	276.9/286.96
R12	FO	*Lamprocyrtis heteroporos*	6.6			30X-7, 22–23/32X-1, 20–21	276.42/286.7
D17	FO	*Thalassiosira jacksonii*	6.5–6.6			32X-3, 46/32X-CC	288.46/296.20
D18	FO	*Neodenticula kamtschatica*	7.1–7.2			35X-CC/36X-CC	325.1/334.8
D19	FO	*Nitzschia reinholdii*	7.2–7.3			32X-CC/35X-CC	296.2/325.10
D20	LO	*Thalassionema schraderi*	7.4			35X-CC/36X-CC	325.1/334.8
R13		*S. delmontensis* > *S. peregrina*	7.55			35X-1, 22–23/36X-1, 29–30	315.62/325.39
R14	LO	*Prunopyle hayesi*	7.6			35X-1, 22–23/36X-1, 29–30	315.62/325.39
R15	FO	*Stylacontarium acquilonium*	7.7			35X-1, 22–23/36X-1, 29–30	315.62/325.39

Notes: R = radiolarian, D = diatom, B = base, T = top, FO = first occurrence, LO = last occurrence, LCO = last common occurrence, and > = transition.

in low abundance at several intervals, whereas diatoms are common to abundant, and are well preserved throughout the entire sequence. Radiolarians occur throughout the section where they are common to abundant in most Quaternary sediments, and rare in Miocene and Pliocene sequences. Only a few samples contained minor amounts of reworked fauna.

The magnetostratigraphy at Site 882 (Shipboard Scientific Party, 1993b; Weeks et al., this volume) extends down through the Gilbert Reversed-Polarity Chron, although the separate polarity boundaries of the Gauss Normal-Polarity Chron and the upper normal event of the Gilbert Reversed-Polarity Chron are only tentatively identified. The estimated ages of paleomagnetic polarity boundaries and diatom, radiolarian, and calcareous nannofossil datum levels recorded in sediments recovered from Holes 882A and 882B, the interval over which they occur, and the depth of this interval in mbsf are given in Table 2.

An age vs. depth curve was plotted in Figure 3 based primarily on magnetostratigraphic polarity boundaries (Table 2). However, the reader is referred to Tiedemann and Haug (this volume) where a detailed astronomically-tuned time scale is presented. The presence of the diatom *Thalassiosira miocenica* in Sample 145-882A-42H-CC, the stratigraphically lowest sample taken at Site 882, implies that the base of Hole 882A is younger than 6.3 Ma (latest Miocene), consistent with the magnetic polarity interpretation shown in Figure 3.

Site 883

Site 883 was drilled on the top of Detroit Seamount (51°11.9′N, 167°46.1′E; 2396 m water depth), 49 nautical miles (nmi) to the north of Site 882. Drilling at Site 883 penetrated an 820-m-thick sequence of Cenozoic sediments overlying a thin sequence of Cretaceous sediments before reaching basement at about 840 mbsf. The 655-m-thick section of Miocene to Pleistocene sediments is rich in well-preserved siliceous microfossils, diatoms being the most abundant. The calcareous microfossil abundance is highly variable. The diversity of the calcareous nannofossils is low, and few biostratigraphic datums were identified in the Pleistocene. The Miocene to Pleistocene biostratigraphy is essentially based on siliceous microfossils, which are much more diverse than the calcareous microfossils (Table 3).

The magnetostratigraphy, obtained on board ship at Site 883, extends down to the Gauss Normal-Polarity Matuyama Reversed-Po-

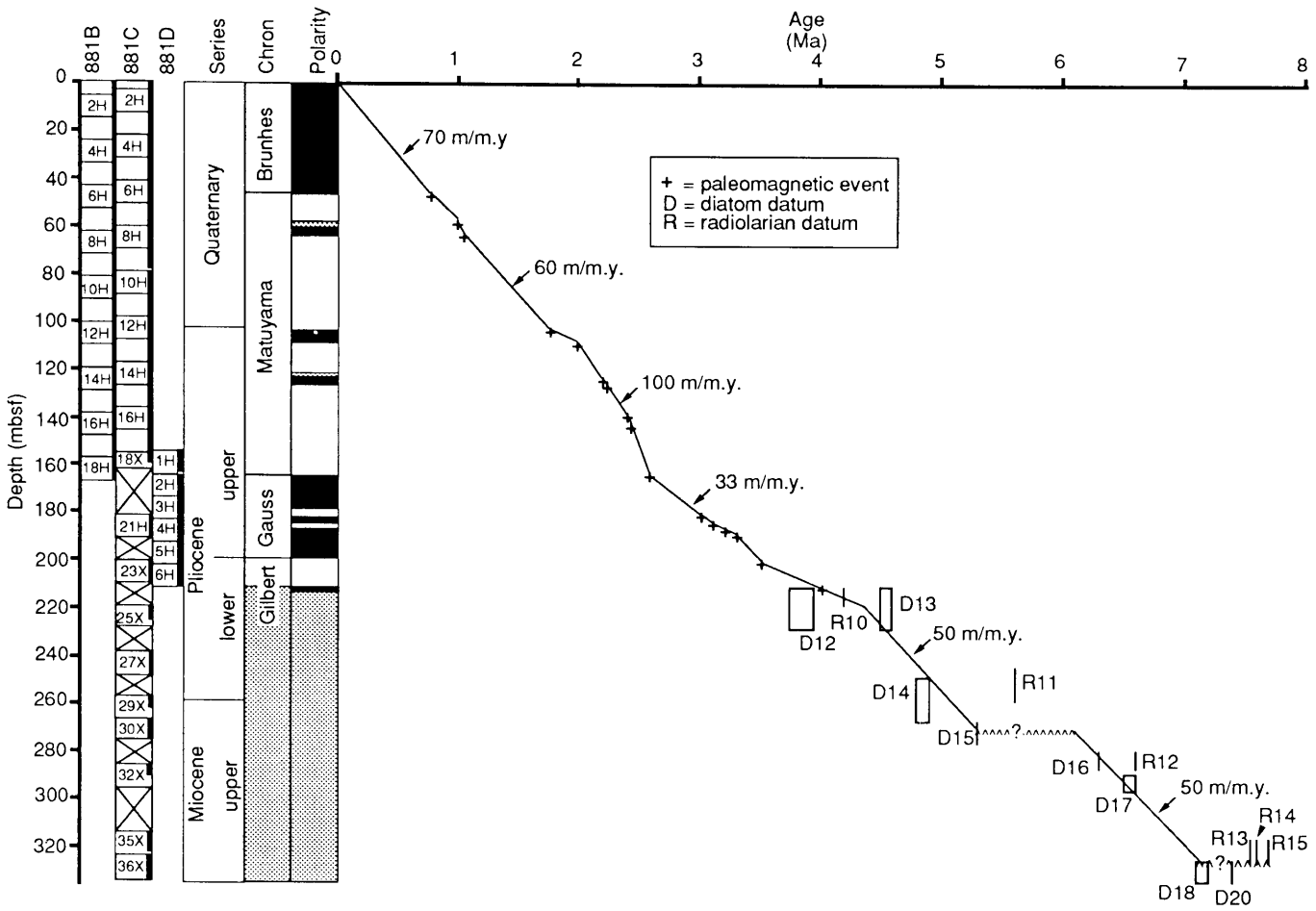

Figure 2. Age vs. depth plot of Site 881 after Table 1. Wavy line = inferred unconformity. Interval and recovery (in black) of cores taken in Holes 881B, 881C, and 881D are shown to the left along with magnetostratigraphy.

larity Chron boundary (Shipboard Scientific Party, 1993c; Weeks et al., this volume); sample magnetization below this level being too weak for the ship's pass-through magnetometer. Additional work on discrete samples, after the cruise, led to an extension of this lower limit down to Subchron C3n.3n of the Gilbert Reversed-Polarity Chron (S. Leroux, 1993; G. Dubuisson, unpubl. data., 1993) (Table 3; Fig. 4).

The Paleogene sediments contain abundant calcareous nannofossil assemblages. Almost no diatoms were observed in this part of the record. Radiolarians are either present in low abundances (rare and very rare) or are absent in all but a few pre-Miocene samples. Calcareous foraminifers are common, although preservation deteriorates from moderate to poor through the Paleogene. The stratigraphy is based on the calcareous nannofossil, planktonic foraminifer, benthic foraminifer, and oxygen isotope data (Table 3), but the Paleogene section is not complete.

Cores 883B-86X and 883B-87X contain the calcareous nannofossil *Ceratolithus aculeus* which implies a Campanian or Maestrichtian age; however, the presence of a few specimens of *Lithraphidites* cf. *quadratus* in Sample 145-883B-86X-4, 90–91 cm suggests a late Maestrichtian age (Beaufort and Ólafsson, this volume).

Unconformities

Age vs. depth curves are plotted for the younger section (middle Miocene to Quaternary) and the older section (Upper Cretaceous to middle Miocene) of Site 883 in Figures 4 and 5, respectively. The entire late middle Miocene, as well as the earliest late Miocene (ca. 14.2–10.2 Ma), is condensed within or removed from the interval between Sample 145-883B-59X-2, 22–23 cm (558.72 mbsf) and the base of Core 145-883B-57X (547.1 mbsf; Table 3; Fig. 4). Within this interval, Sample 145-883B-58X-CC contains a diatom assemblage assignable to the *Denticulopsis praedimorpha* Zone (12.8–11.4 Ma; Barron and Gladenkov, this volume), but unfortunately only 0.83 m was recovered in Core 145-883B-58X. An attempt to recover this compressed interval in Core 145-883E-1R (547.0–556.5 mbsf) failed because the top of the 6.15-m-thick section, recovered in that core, correlates with the *Denticulopsis hyalina* Zone and is older than 13.1 Ma. Thus, either a greatly condensed interval or two hiatuses—one removing the *Thalassiosira yabei* Zone (11.4–9.8 Ma) and the other removing the *Crucidenticula nicobarica* Zone (13.1–12.8 Ma)—must be present at Site 883.

Stratigraphic horizons in Holes 883B and 883F, the hole drilled for logging, apparently are at equivalent depths so that logging results can be related directly to the cores studied for biostratigraphy and magnetostratigraphy. The natural gamma-ray logs for potassium, thorium, and aluminum identify a short clay-rich interval between about 530 and 550 mbsf in Hole 883F. This clay-rich interval gives rise to a sharp peak in core susceptibility between about 538 and 550 mbsf where values (ppm) are three to four orders of magnitude higher than those in the surrounding interval. Seismic stratigraphic data indicate a change in sedimentation at this depth (Hamilton, this vol-

Table 2. Age, interval, and depth of magnetostratigraphic polarity boundaries and biostratigraphic datum levels in Holes 882A and 882B.

		Datum	Age (Ma)	Core, section, interval (cm) 145-882A-	Depth (mbsf)	Core, section, interval (cm) 145-882B-	Depth (mbsf)
R1	LO	*Lychnocanoma nipponica sakaii*	0.05	Above 1H-CC	Above 8.8	Above 1H-CC	above 4.4
D1	LO	*Simonseniella curvirostris*	0.3	1H-CC/2H-CC	8.8/18.3	1H-CC/2H-CC	4.4/13.9
R2	LO	*Stylacontarium acquilonium*	0.35	1H-CC/2H-CC	8.8/18.3	2H-CC/3H-CC	13.9/23.4
N1	LO	*Pseudoemiliania lacunosa*	0.493			3H-CC/4H-CC	23.4/32.9
R3	LO	*Stylatractus universus*	0.55	2H-CC/3H-CC	18.3/27.8	2H-CC/3H-CC	13.9/23.4
	B	C1n.1n	0.78	4H-4, 120	35.5	5H-1, 40	35.3
	T	C1r.1n	0.98	5H-6, 0–52	44.8–45.32	6H-2, 80	44.7
D2	LCO	*Actinocyclus oculatus*	1.0	4H-CC/5H-CC	37.3/46.8	5H-CC/6H-CC	42.4/51.9
R4	LO	*Eucyrtidium matuyamai*	1.0	5H-CC/6H-CC	46.8/56.3	6H-CC/7H-CC	51.9/61.4
	B	C1r.1n	1.049	6H-2, 10	48.4		
D3	FO	*Simonseniella curvirostris*	1.58	7H-CC/8H-CC	65.8/75.3	8H-CC/9H-CC	70.9/80.4
	T	C2n.1n	1.757	9H-1, 10	75.4		
	B	C2n.1n	1.98	9H-2, 135	78.15		
R5	FO	*Eucyrtidium matuyamai*	2.0	8H-CC/9H-CC	75.3/84.8	9H-CC/10H-CC	80.4/89.9
D4	LO	*Neodenticula koizumii*	2.0–2.1	8H-CC/9H-CC	75.3/84.8	9H-CC/10H-CC	80.4/89.9
	T	C2r.1n	2.20	9H-6, 25	83.05		
	B	C2r.1n	2.23	9H-6, 85	83.65		
	T	C2An.1n	2.60	11H-3, 80	98.1		
D5	LCO	*Neodenticula kamtschatica*	2.63–2.7	11H-CC/12H-CC	103.8/113.3	11H-CC/12H-CC	99.4/108.9
D6	FO	*Neodenticula seminae*	2.7	11H-CC/12H-CC	103.8/113.3	11H-CC/12H-CC	99.4/108.9
N2	LO	Small *Reticulofenestra*	2.75			13H-CC/14H-CC	118.4/127.9
R6	FO	*Cycladophora davisiana davisiana*	2.9			13H-CC/14H-CC	118.4/127.9
	B	C2An.1n?	3.054?		146.5		
D7	LO	*Thalassiosira marujamica*	3.1–3.2	16H-CC/17H-CC	151.3/160.8	17H-CC/18H-CC	156.4/165.9
	B	C2An.2n?	3.221?		165.5		
D8	FO	*Neodenticula koizumii*	3.51–3.85	19H-CC/20H-CC	179.8/189.3	19H-CC/20H-CC	175.4/184.9
	B	C2An.3n?	3.553?		202.0		
D9	FO	*Actinocyclus oculatus*	3.65–3.85	21H-CC/22H-CC	198.8/208.3	20H-CC/21H-CC	184.9/194.4
	T	C3n.1n	4.033		267.0		
	B	C3n.1n	4.134		279.0		
	T	C3n.2n	4.265		302.0		
	B	C3n.2n	4.611		317.0		
D10	LO	*Thalassiosira jacksonii* (plicate)	4.5–4.6	34H-CC/35H-CC	322.3/331.8		
	T	C3n.3n	4.694		329.0		
	B	C3n.3n	4.611		336.0		
	T	C3n.4n	4.812		342.0		
D11	FO	*Thalassiosira latimarginata* s.str.	4.8–4.9	36H-CC/37H-CC	341.3/350.8		
	B	C3n.4n	5.046		357.0		
D12	FO	*Thalassiosira oestrupii*	5.3	39H-CC/40H-CC	369.8/379.3		
D13	LO	*Thalassiosira miocenica*	5.7	40H-CC/41H-CC	379.3/388.8		
D14	FO	*Thalassiosira miocenica*	6.2	Below 42H-CC	>398.8		

Note: Abbreviations as in Table 1, with the addition of N = calcareous nannofossil.

ume) from a flat-based wedge below, thickening toward an upslope source that lies to the southwest, to an overlying hemipelagic unit that dips and thickens downslope to the northeast and exhibits gentle drape folds. A similar upper middle Miocene interval is also missing or is greatly condensed at Gulf of Alaska DSDP Site 183 (Barron, 1989).

A possible second unconformity between the lower Oligocene section (>30 Ma) and the middle part of the lower Miocene section (ca. 21 Ma; Fig. 5) may be present at the sharp lithologic break between greenish-gray, diatom-rich, calcareous chalk above and light-brownish-gray, diatom-poor, calcareous chalk below (lithologic Units III and IV, respectively) at 652.2 mbsf. Alternatively, the upper lower Oligocene through lowermost Miocene section of Cores 883B-69X and 883B-70X may be greatly condensed with sediment accumulation rates of 2 m/m.y. or less (Fig. 5). An abrupt rise in weight-percent potassium and aluminum, according to the geochemical log and the abrupt decline in diatoms at this interval, occur downhole at the level of the lithologic break (Shipboard Scientific Party, 1993c), indicating a change in sedimentation style. Seismic stratigraphy, however, does not recognize a break at this depth (Hamilton, this volume).

A third unconformity is recognized by nannofossil stratigraphy (Beaufort and Ólafsson, this volume) at about 710 mbsf within the unrecovered interval between Cores 145-883B-74X and 883B-75X (Fig. 5). Here, middle Eocene sediments dated by biostratigraphy at about 42 Ma (calcareous nannofossil Zone NP 16) are overlain by lowermost Oligocene sediments (calcareous nannofossil Zone NP 22). Rare to common middle to upper Eocene radiolarians of the *Dictyoprora amphora* Zone are present below the unconformity, whereas sediments immediately overlying the unconformity are barren of radiolarians (Shilov, this volume). Although no lithologic or seismic stratigraphic breaks are recorded at this interval, percent $CaCO_3$ decreases and magnetic susceptibility increases abruptly down-section at about 710 mbsf, indicating a possible change in sedimentation style (Shipboard Scientific Party, 1993c; Hamilton, this volume).

A fourth possible unconformity at the lower Eocene/middle Eocene boundary at about 780 mbsf (in the unrecovered interval between Cores 145-883B-81X and 883B-82X) is suggested by planktonic foraminifer stratigraphy (Basov, this volume; Fig. 5) and the apparent absence of calcareous nannofossil subzone NP 14a (Beaufort and Ólafsson, this volume). The nannofossil datum levels used in the age vs. depth curve (Fig. 5) imply that any hiatus at this depth would be brief (ca. 50.5–49.3 Ma); however, use of alternative age estimates from Wei and Peleo-Alampay (1993) for the first occurrence (FO) of *Discoaster sublodoensis* (49.6 Ma) and the last occurrence (LO) of *Tribrachiatus orthostylus* (50.5 Ma; Table 3) would reduce the "kink" in the age vs. depth curve (Fig. 5) and reduce the likelihood of a hiatus. Although no lithologic break was recorded at this interval, percent $CaCO_3$, dry-bulk density, and magnetic susceptibility increase abruptly down section at about 780 mbsf, indicating a possible change in sedimentation style (Shipboard Scientific Party, 1993c).

An unconformity or interval of greatly condensed sediments at the Paleocene/Eocene boundary in the lower part of Core 883B-85X between 813.1 and 813.5 mbsf is suggested by the absence of calcareous nannofossil zone NP 10 (Beaufort and Ólafsson, this volume; Pak and Miller, this volume). This 40-cm-thick interval represents 3 m.y. of deposition (55–52 Ma; Fig. 5) and corresponds with a dark-brown clayey sandstone layer within nannofossil chalk (Shipboard Scientific Party, 1993c).

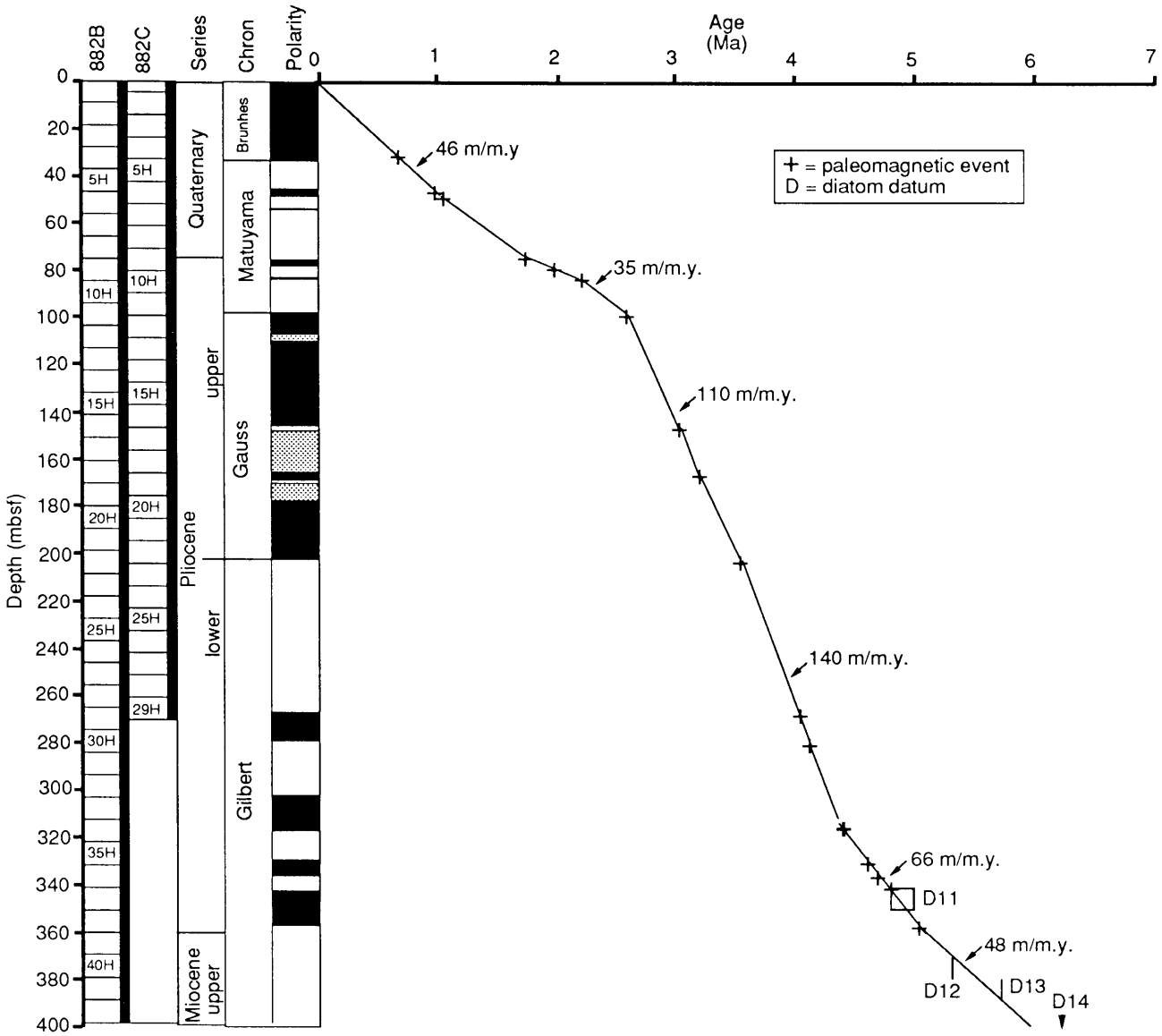

Figure 3. Age vs. depth plot of Site 882 after Table 2.

A major unconformity between Maestrichtian and uppermost Paleocene sediments is present in the unrecovered interval between the base of Core 145-883B-85X and the top of Core 145-883B-84X (814–818.5 mbsf; Fig. 5). This break coincides with the contact between lithologic Unit V, yellow green and yellow brown to reddish-brown ashes, and lithologic Unit IV, nannofossil ash and chalk (Shipboard Scientific Party, 1993c). Abrupt downhole increases in the natural gamma-ray logs for potassium and uranium are recorded at this interval (Shipboard Scientific Party, 1993c). Seismic stratigraphic data indicate that lithologic Unit V fills a local depression that is 3.4 km across on the top of the basalt of Detroit Seamount (Hamilton, this volume).

Site 884

Drilling at Site 884 on the east flank of Detroit Seamount (51°27′N, 168°20.2′E; 3836 m water depth) recovered an 850-m-thick sequence of upper Paleocene(?) through Pleistocene sediments in five holes (Shipboard Scientific Party, 1993d). The Neogene and Pleistocene are represented by a 640-m-thick section of diatomite, claystone, and clayey diatom ooze. Calcareous microfossil abundance is highly variable throughout this interval. A limited nannofossil zonation was possible for the Quaternary part of the section.

In general, diatoms are abundant to common and well preserved to moderately well preserved throughout the upper Oligocene through Quaternary section cored above 658 mbsf at Site 884 (see also Gladenkov and Barron, this volume). Radiolarians are abundant only in the middle Miocene part of the section and in three isolated samples from the upper Miocene, upper Pliocene, and lower Pleistocene parts of the section.

An added bonus of drilling at Site 884 was the retrieval of an excellent paleomagnetic stratigraphy in the upper 560 m of Hole 884B, which extends from the Pleistocene back to at least the early middle Miocene or more (Table 4; Fig. 6). In addition, Dubuisson et al. (this volume) used down-hole magnetic logs to recognize magnetic polarity boundaries in the upper 440 m of Hole 884E (Table 6).

Recognition of magnetic-polarity subchrons C1n through C5n (0–10.8 Ma) is straightforward, and good agreement exists between the ages suggested by diatoms and radiolarians (Barron and Gladenkov, this volume; Morley and Nigrini, this volume) and the paleomagnetic

Table 3. Age, interval, and depth of magnetostratigraphic polarity boundaries and biostratigraphic datum levels in Hole 883B.

		Datum	Age (Ma)	Core, section, interval (cm) 145-883B-	Depth (mbsf)
R1	LO	*Lychnocanoma nipponica sakaii*	0.05	Above 1H-CC	above 7.9
N1	FO	*Emiliania huxleyi*	0.294	1H-5, 130-131/1H-CC	7.30/7.9
D1	LO	*Simonseniella curvirostris*	0.3	1H-CC/2H-CC	7.9/17.4
R2	LO	*Stylacontarium acquilonium*	0.4	1H-CC/2H-CC	7.9/17.4
R3	LO	*Stylatractus universus*	0.55	2H-CC/3H-CC	17.4/26.9
N2	LO	*Pseudoemiliania lacunosa*	0.493	3H-5, 46–47/3H-6, 46–47	23.86/25.36
	B	C1n.1n	0.78	4H-5, 50	33.30
	T	C1r.1n	0.984	5H-5, 120	43.50
D2	LCO	*Actinocyclus oculatus*	1.0	4H-CC/5H-CC	36.4/45.9
	LO	*Eucyrtidium matuyamai*	1.0	5H-CC/6H-CC	45.9/55.4
	B	C1r.1n	1.049	6H-1, 100	47.00
N3	LO	*Calcidiscus macintyrei*	1.538	7H-7, 46–47/7H-CC	64.86/64.9
D3	FO	*Simonseniella curvirostris*	1.58	6H-CC/7H-CC	55.4/64.9
N4	FO	*Gephyrocapsa oceanica*	1.674	7H-CC/8H-1, 46–47	64.9/65.36
	T	C2n.1n	1.757	8H-2, 70	67.1
D4	LO	*Neodenticula koizumii*	1.9–2.0	6H-CC/7H-CC	55.4/64.9
	B	C2n.1n	1.983	8H-4, 60	70
R4	FO	*Eucyrtidium matuyamai*	2.0	7H-CC/8H-CC	64.9/74.4
	T	C2An.1n	2.60	9H-7 to 10H-1	83.7–84.3
D5	LCO	*Neodenticula kamtschatica*	2.63–2.7	9H-CC/10H-CC	83.9/93.4
D6	FO	*Neodenticula seminae*	2.7	9H-CC/10H-CC	83.9/93.4
R5	FO	*Cycladophora davisiana davisiana*	2.9	12H-CC/13H-CC	112.4/121.9
	B	C2An.1n *	3.054		125.15
	T	C2An.2n *	3.127		133.9
D7	LO	*Thalassiosira marujamica*	3.1–3.2	15H-2, 91/15H-2, 135	133.81/134.25
	B	C2An.2n *	3.221		141.45
	T	C2An.3n *	3.325		154.9
N5	LO	*Reticulofenestra pseudoumbilica*	3.713	16H-2, 46–47/16H-3, 46–47	142.86/144.36
D8	FO	*Neodenticula koizumii*	3.51–3.85	18H-CC/19H-CC	159.9/168.4
	B	C2An.3n *	3.553		170.4 (180)
D9	FO	*Actinocyclus oculatus*	3.65–3.85	20H-CC/21H-CC	178.9/188.4
	T	C3n.1n *	4.033		231.65 (219)
	B	C3n.1n *	4.134		241.45 (226)
	T	C3n.2n? *	4.265		266.2
	B	C3n.2n? *	4.432		277.95
	T	C3n.3n *	4.611		287.45
D10	LO	*Thalassiosira jacksonii* (plicate)	4.5–4.6	30H-CC/31H-CC	283.4/292.9
D11	FO	*Thalassiosira latimarginata*	4.9–5.0	31H-CC/32X-CC	292.9/302.5
D12	FO	*Thalassiosira oestrupii*	5.3	33X-CC/34X-CC	312.2/321.9
D13	LO	*Thalassiosira miocenica*	5.7	34X-CC/35X-CC	321.9/331.5
D14	FO	*Thalassiosira praeoestrupii*	5.95	34X-CC/35X-CC	321.9/331.5
D15	FO	*Thalassiosira miocenica*	6.2	44X-CC/45X-CC	419.2/429.0
D16	FO	*Thalassiosira jacksonii*	6.5–6.6	46X-CC/47X-CC	439.3/448.7
R6	FO	*Lamprocyrtis heteroporos*	6.6	33X-CC/34X-CC?	312.2/321.9?
D17	FO	*Neodenticula kamtschatica*	7.1–7.2	49X-CC/50X-CC	468.1/477.9
D18	FO	*Nitzschia reinholdii*	7.2–7.3	50X-CC/51X-CC	477.9/487.9
D19	LO	*Thalassionema schraderi*	7.4	45X-CC/46X-CC	429.0/438.9
R7	FO	*Stylacontarium acquilonium*	7.7	46X-CC/47X-CC	439.3/458.2
R8		*S. delmontensis* > *S. peregrina*	7.55	47X-CC/48H-CC	448.7/458.2
D20	LCO	*Denticulopsis hustedtii*	8.4	53X-CC/54X-2, 104	507.6/510.14
R9	LO	*Lychnocanoma nipponica magnacornuta*	8.8	54X-CC/55X-CC	517.4/527.2
D21	LO	*Denticulopsis dimorpha*	9.0	57X-4, 104/57X-CC	542.64/547.1
D22	FO	*Denticulopsis dimorpha*	9.8	57X-CC/58X-CC	547.1/557.0
D23	LCO	*Denticulopsis praedimorpha*	11.4	58X-CC/59X-CC	557.0/567.0
R10	LO	*Cyrtocapsella cornuta*	11.7	58X-CC/59X-CC	557.0/567.0
R11	FO	*Lychnocanoma nipponica magnacornuta*	12.5	57X-CC/58X-CC	547.1/557.0
D24	FO	*Denticulopsis praedimorpha*	12.8	58X-CC/59X-2, 22	557.0/558.72
D25	FCO	*Denticulopsis hustedtii*	13.1	58X-CC/59X-2, 22	557.0/558.72
N6	LO	*Sphenolithus heteromorphus*	13.51	62X-6, 46–47/62X-7, 46–47	594.96/596.46
D26	FO	*Denticulopsis hustedtii*	14.2	58X-CC/59X-2, 22	557.0/558.72
D27	FO	*Denticulopsis hyalina*	14.9	60X-CC/61X-2, 104	577.0/579.54
R12	FO	*Eucyrtidium inflatum*	15.3	61X-CC/62X-CC	587.0/597.0
D28	FO	*Denticulopsis lauta*	15.9	62X-CC/63X-2, 104	597.0/599.54
D29	FO	*Denticulopsis praelauta*	16.3	63X-2, 104/63X-4, 104	599.54/602.54
N7	FO	*Sphenolithus heteromorphus*	18.18	65X-2, 46–47/65X-3, 46–47	618.66/620.06
D30	FO	*Crucidenticula sawamurae*	18.4	65X-CC/66X-2, 104	626.3/628.84
N8	O	*Sphenolithus belemnos*	18.54–19.19	66X-2, 46–47	628.26
D31	FO	*Thalassiosira fraga*	20.1	68-4, 22/68X-CC, 3	649.87/652.13
R13	FO	*Cyrtocapsella tetrapera*	22.6	67X-CC/68X-CC	645.1/654.8
D32	O	*Lisitzinia ornata*	24.3–27.9	68X-CC	654.8
N9	LO	*Dictyococcites bisectus*	23.81	69X-2, 46–47/69X-3, 46–47	656.76/658.26
D33	FO	*Cavitatus miocenica*	30.6	69X-CC/70X-CC	664.4/674.1
N10	LO	*Reticulofenestra umbilica*	31.72 (32.4)	71X-1, 46–47/71X-2, 46–47	674.56/676.06
N11	LO	*Isthmolithus recurvus*	32.5	71X-7, 46–47/71X-CC	683.56/683.7
N12	LO	*Ericsonia formosa*	32.7 (32.9)	74X-CC/75X-1, 45–46	705.99/713.06
IS		Oxygen isotope increase	34.3	74X-2, 95–100/75X-1, 30–35	705.45/712.80
N13	LO	*Discoaster saipanensis*	34.98 (34.2)	74X-CC/75X-1, 45–46	705.99/713.06
N14	LO	*Discoaster barbadiensis*	34.98 (34.2)	74X-CC/75X-1, 45–46	705.99/713.06
N15	FO	*Isthmolithus recurvus*	35.08 (36.2)	74X-CC/75X-1, 46–47	705.99/713.06
N16	LO	*Chiasmolithus grandis*	(37.1)	74X-CC/75X-1, 46–47	705.99/713.06
N17	LO	*Chiasmolithus solitus*	39.72	74X-CC/75X-1, 46–47	705.99/713.06
P1	LO	*Acarinina bullbrooki*	40.5	74X-2, 120–122/75X-1, 120–122	705.7/713.8
P2	FO	*Globigerinatheka index*	42.9	75X-1, 120–122/75X-2, 45–47	713.8/714.55
N18	LO	*Discoaster distinctus*		75X-5, 46–47/76X-1, 46–47	719.06/721.56
N19	FO	*Discoaster bifax*	(43.7)	76X-4, 46–47/76X-5, 46–47	725.06/726.56

Table 3 (continued).

		Datum	Age (Ma)	Core, section, interval (cm) 145-883B-	Depth (mbsf)
N20	O	*Chiasmolithus gigas*	(44.6–46.3)	76X-6, 46–47	728.06
P3	FO	*Acarinina bullbrooki*	45.2	78X-2, 120–122/78X-5, 123–125	740.4/746.93
N21	LO	*Discoaster sublodoensis*	47.23	78X-CC/79X-1, 46–47	749.5/749.96
N22	LO	*Nannotetrina fulgens*	(47.3)	79-CC/80-CC	754.5/769.2
N23	FO	*Nannotetrina cristata*	47.8	80X-CC/81X-CC	769.2/779.2
N24	LO	*Discoaster lodoensis*	47.9	80X-CC/81X-CC	769.2/779.2
N25	FO	*Discoaster sublodoensis*	49.29 (49.6)	81X-CC/82X-1, 46–47	779.2/779.66
N26	LO	*Tribrachiatus orthostylus*	50.78 (50.5)	82X-3, 46–47/82X-4, 46–47	782.66/784.16
P4	FO	*Acarinina pentacamerata*	50.8	83X-3, 120–122/83X-4, 122–124	793.4/794.92
N27	FO	*Discoaster lodoensis*	52.04 (52.5)	85X-2, 140–141/85X-3, 20–21	811.80/812.10
P5	FO	*Morozovella aragonensis*	52.3	83X-CC/84X-1, 60–62	795.27/799.8
N28	FO	*Tribrachiatus orthostylus*	53.32	85X-3, 120–121/85X-3, 140–141	813.10/813.30
N29	LO	*Fasciculithus tympaniformis*	54.08	85X-3, 140–141/85X-4, 4–5	813.30/813.44
BF		Benthic extinction event	55.3	85X-3, 129–134/85X-4, 10–15	813.19/813.50
N30	FO	*Discoaster multiradiatus*	(56.5)	85X-4, 7–8/85X-4, 10–11	813.47/813.50
N31	FO	*Discoaster mohleri*	57.79 (57.9)	85X-CC/86X-1, 110	814.1/819.6
N32	FO	*Heliolithus kleinpellii*	58.57 (59.5)	85X-CC/86X-1, 110	814.1/819.6
N33	FO	*Fasciculithus tympaniformis*	60.63 (60.0)	85X-CC/86X-1, 110	814.1/819.6
N34	LO	*Micula* spp.	65.0 (66.1)	85X-CC/86X-1, 110	814.1/819.6

Notes: Abbreviations as in Table 1, with the addition of N = calcareous nannofossil, P = planktonic foraminifer, IS = oxygen isotope, BF = benthic foraminifer, O = occurrence, and FCO = first common occurrence. Asterisk (*) = after Leroux (1993). Ages in parentheses after Wei and Peleo-Alampay (1993).

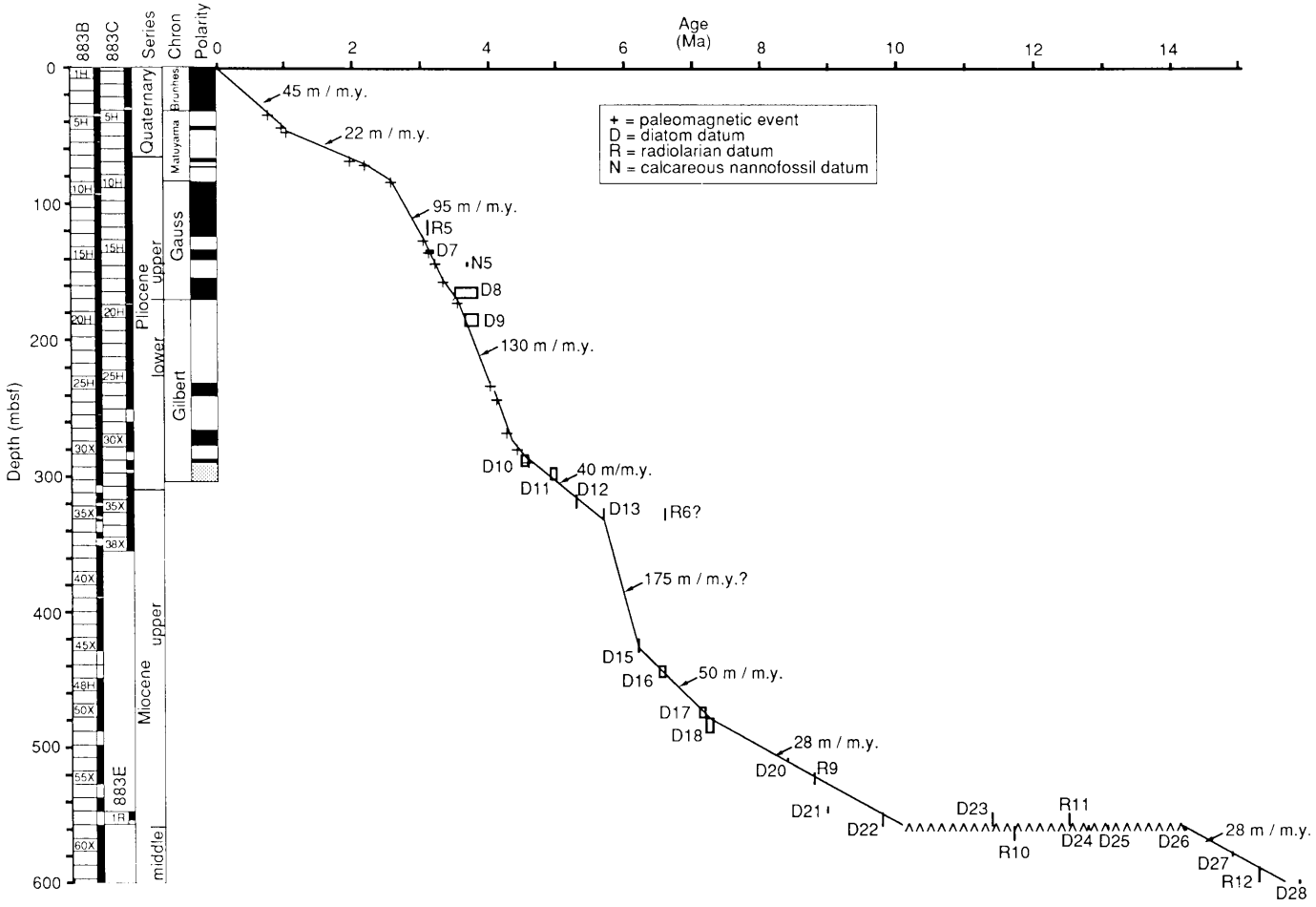

Figure 4. Age vs. depth plot of the middle Miocene through Quaternary section of Site 883 after Table 3.

interpretation of Weeks et al. (this volume; Table 4). Diatom and radiolarian biostratigraphy, however, suggest that sediment accumulation rates decrease markedly beginning down-section in the middle Miocene part of the section (ca. 500 mbsf; Fig. 6), and the magnetostratigraphic interpretation favored by the biostratigraphy for the middle Miocene sequence of Hole 884B is "Interpretation 2" of the Shipboard Scientific Party (1993d) and Weeks et al. (this volume). A few minor modifications, however, are suggested by diatom and radiolarian stratigraphy to "Interpretation 2" (Table 4; Fig. 6). The normal-polarity interval recognized between 535.0 and 542.3 mbsf is inferred to represent combined Subchrons C5AA and C5AB, whereas the normal interval recognized between 550 and 559 mbsf is sug-

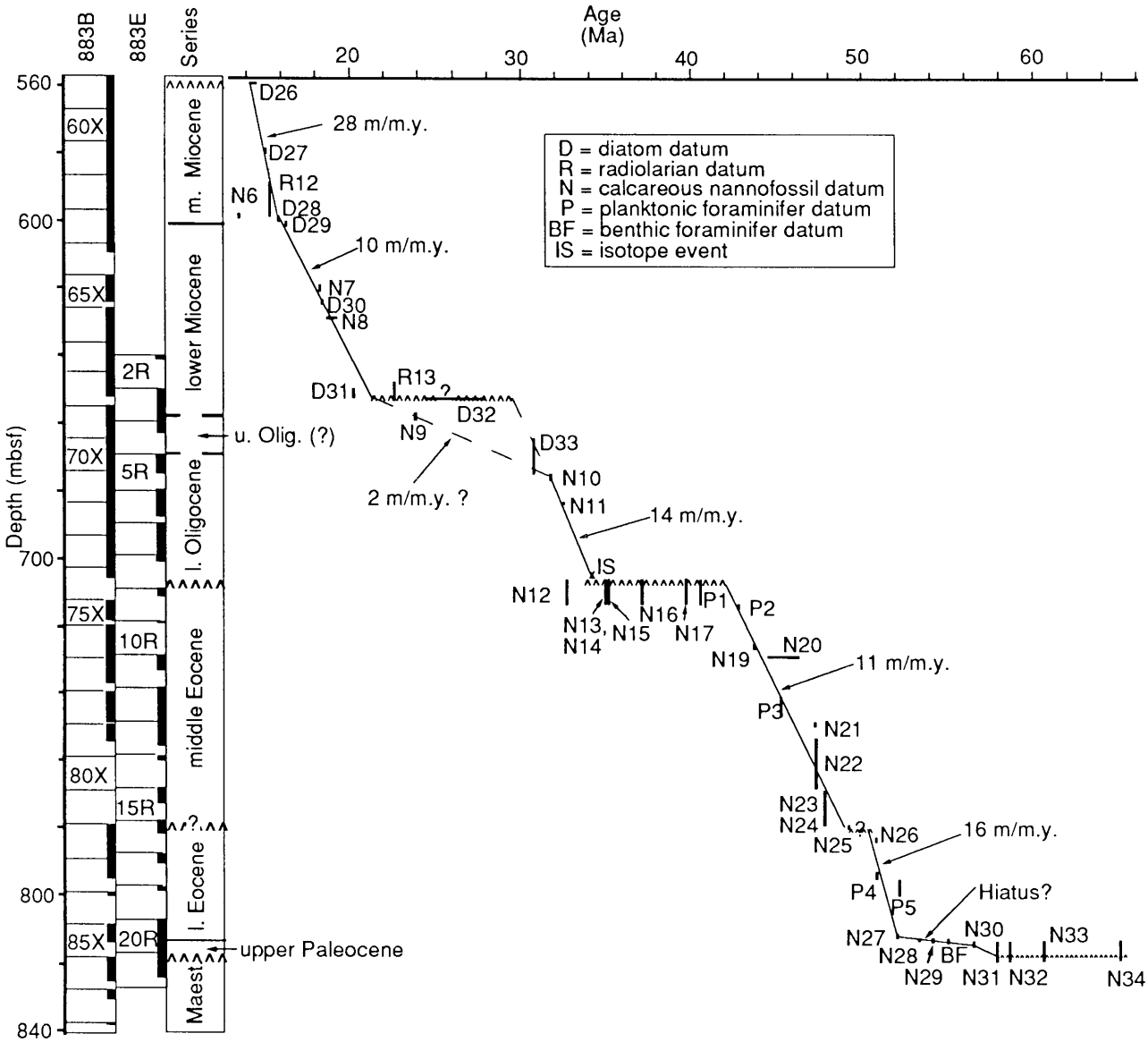

Figure 5. Age vs. depth plot of the Maestrichtian through lower Miocene section of Site 883 after Table 3.

gested to be Subchron C5AD. These modifications are based on calibration of diatom and radiolarian datum levels with magnetostratigraphy at Site 887 (Barron and Gladenkov, this volume; Morley and Nigrini, this volume), where the magnetostratigraphic record is easier to interpret.

Shipboard measurement of inclination from the pass-through cryogenic magnetometer (after 15 mT demagnetization) suggested the possibility of three normal-polarity intervals beginning at 580.0, 594.2, and 602.8 mbsf; however, this part of the record was not interpreted by Weeks et al. (this volume) because of poor data quality. Nevertheless, diatom and radiolarian datum biostratigraphy at Site 887 (Barron and Gladenkov, this volume; Morley and Nigrini, this volume) suggests a tentative correlation of these three possible polarity boundaries with the tops of Chrons C5C, C5D, and C5E, respectively (Table 4; Fig. 6).

On Figure 6, magnetostratigraphic polarity boundaries and biostratigraphic datum levels (Table 4) are used to construct an age vs. depth curve for the middle Miocene to the Quaternary of Site 884. Although the curve is mainly plotted according to magnetostratigraphic polarity boundaries, diatom and radiolarian datum levels in the upper lower Miocene to middle Miocene interval between 600 and 500 mbsf (Table 4) proved to be critical in identifying the various paleomagnetic chrons. These microfossil events can be identified at Site 887 where they are constrained by an excellent magnetostratigraphic record (Barron and Gladenkov, this volume; Morley and Nigrini, this volume; Weeks et al., this volume).

Calcareous nannofossil, planktonic foraminiferal, diatom, and radiolarian datum levels from Table 4, as well as the distinctive late Eocene oxygen isotope increase, are used in Figure 7 to plot an age vs. depth curve for the middle Eocene through lower Miocene section of Site 884. Sediment accumulation rates are relatively low for the older interval of Site 884, with the exception of the upper Eocene part of the section (ca. 769 to 694 mbsf) where rates of 70 m/m.y. are suggested. This upper Eocene interval coincides with lithologic Subunit IIB, a unit of chalk, claystone, and ash, which contains evidence of large-scale redeposition, including slumping and diamictic conglomerates (Shipboard Scientific Party, 1993d). Calcareous nannofossils and planktonic foraminifer biostratigraphy suggest that the interval from Core 145-884B-87X through the greater part of Core 145-884B-83X (814–769 mbsf) lies in the middle Eocene (Beaufort and

Table 4. Age, interval, and depth of magnetostratigraphic polarity boundaries and biostratigraphic datum levels in Holes 884B, 884C, and 884E.

		Datum	Age (Ma)	Core, section, interval (cm) 145-884B-	Depth (mbsf)	Hole 884C depth (mbsf)	Hole 884E depth (mbsf)
R1	LO	*Lychnocanoma nipponica sakaii*	0.05	Above 1H-CC	Above 6.5	2.4/11.9	
D1	LO	*Simonseniella curvirostris*	0.3	1H-CC/2H-CC	6.5/16.0	11.9/21.4	
R2	LO	*Stylacontarium acquilonium*	0.4	2H-5, 135–136/3H-5, 135–136	13.85/23.35	11.9/21.2	
R3	LO	*Stylatractus universus*	0.55	3H-5, 135–136/4H-5, 135–136	23.35/32.85	21.4/30.9	
	B	C1n.1n	0.78		42.5	41.1	
	T	C1r.1n	0.984		54.00–55.10	55.0	
D2	LCO	*Actinocyclus oculatus*	1.0	5H-CC/6H-CC	44.5/54.0	49.9/59.4	
R4	LO	*Eucyrtidium matuyamai*	1.0	6H-5, 135–136/7H-5, 135–136	51.85/61.3	559.4/68.9	
R5	FO	*Eucyrtidium matuyamai*	2.0	12X-1, 68–69/13X-3, 134–135	87.98/97.64	78.4/88.2	
	B	C1r.1n	1.049		59.4	59.7	
D3	FO	*Simonseniella curvirostris*	1.58	11H-CC/12X-CC	87.3/93.3	88.2/97.8	
R6	LO	*Sphaeropyle robusta*	1.5–1.7	10H-CC/12X-1, 68–69	86.3/87.98		
	T	C2n.1n	1.757	?	?	?	97.14
	B	C2n.1n	1.983		96.9	101.9	102.78
D4	LO	*Neodenticula koizumii*	1.9–2.1	13X-4, 54/14X-4, 47	98.34/108.97	97.8/107.4	
	T	C2r.1n	2.197		107.1		107.52
	B	C2r.1n	2.229		108.2		108.42
	T	C2An.1n	2.60		121.30–122.50	118.50–127.00	123.98
D5	LCO	*Neodenticula kamtschatica*	2.63–2.7	15X-CC/16X-CC	122.2/131.8	136.3/146.0	
D6	FO	*Neodenticula seminae*	2.7	15X-CC/16X-CC	122.2/131.8	136.3/146.0	
R7	FO	*Cycladophora davisiana*	2.9	17X-5, 135–136/18X-5, 135–136	139.15/148.85	136.3/146.0	
	B	C2An.1n	3.054		148.1	147.00–147.80	149.57
	T	C2An.2n	3.127		152.35	154.50–156.00	154.61
D7	LO	*Thalassiosira marujamica*	3.1–3.2	18X-CC/19X-CC	151.0/160.8	155.7/165.3	
	B	C2An.2n	3.221		159.5–159.7	158.5–159.5	160.26
	T	C2An.3n	3.325			164.4	167.87
	B	C2An.3n	3.553		179.2	178.0	179.59
D8	FO	*Neodenticula koizumii*	3.51–3.85	23X-5, 25/23X-CC	196.05/199.4	194.3/204.0	
D9	FO	*Actinocyclus oculatus*	3.65–3.85	24X-5, 25/24X-CC	205.65/209.1	204.0/213.7	
	T	C3n.1n	4.033		219.65	218.45	218.77
	B	C3n.1n	4.134		224.2	224.5	224.71
	T	C3n.2n	4.265			235.9	237.77
	B	C3n.2n	4.432			244.25	246.49
D10	LO	*Thalassiosira jacksonii* (plicate)	4.5–4.6	29X-CC/30X-2, 25	252.4/259.05	261.8/271.4	
	T	C3n.3n	4.611		252.1?	251.5–252.4	254.28
	B	C3n.3n	4.694		258.4?	256.9	258.23
	T	C3n.4n	4.812		266.3–267.2	261.8–261.9	262.96
D11	FO	*Thalassiosira latimarginata* s.str.	4.8–4.9	31X-2, 25/31X-5, 25	268.75/273.25	271.4/281.1	
	B	C3n.4n	5.046		276.5–276.9	275.23	
D12	FO	*Thalassiosira oestrupii*	5.3	33X-2, 25/33X-5, 25	288.05/292.55	281.1/290.7	
	T	C3An.1n	5.705		311.55	311.43	
D13	FO	*Thalassiosira praeoestrupii*	5.95	36X-5, 25/36X-CC	321.55/325.03	19.7/329.2	
	B	C3An.1n	5.946		324.8–325.2	325.7	324.37
	T	C3An.2n	6.078		334.5	332.4	333.07
D14	FO	*Thalassiosira miocenica*	6.2	38X-2, 25/38X-5, 25	336.05/340.55	338.7/348.2	
	B	C3An.2n	6.376		348.00	348.2	348.76
	T	C3Bn	6.744		364.0–364.6		366.6
	B	C3Bn	6.901		367.6		369.79
	T	C3Br.1n	6.946		369.1		370.87
	B	C3Br.1n	6.981		370.25		372.28
D15	FO	*Neodenticula kamtschatica*	7.1–7.2	41X-CC/42X-2, 26	372.7/374.46		
	T	C4n.1n	7.245		374.2		376.81
	B	C4n.1n	7.376		379.65		381.98
D16	LCO	*Thalassionema schraderi*	7.4	42X-5, 25/42X-CC	378.95/382.4		
	T	C4n.2n	7.464		381.5		385.95
R8	LO	*Prunopyle hayesi*	7.6	43X-5, 135–136/45X-5, 135–136	389.9/409.1		
R9	FO	*Stylacontarium acquilonium*	7.7	43X-5, 135–136/45X-5, 135–136	389.9/409.1		
	T	C4n.2n	7.892		400.2		398.02
	B	C4r.1n	8.047				404.7
	B	C4r.1n	8.079				405.14
D17	LCO	*Denticulopsis katayamae*	8.4	46X-3, 25/46X-4, 25	414.45/416.05		
	T	C4An.1n	8.529		418.45		424.97
R10	LO	*Lychnocanoma nipponica magnacornuta*	8.8	47X-5, 135–136/48X-5, 135–136	428.3/438.0		
	B	C4An.1n	8.861		436.15		438.75
D18	LO	*Denticulopsis dimorpha*	9.0	48X-6, 25/48X-CC	438.35/440.2		
	T	C4Ar.1n	9.069		440.65		
	T	C4Ar.1n	9.149		445.2		
	T	C4r.2n	9.428		451.1?		
	B	C4r.2n	9.491		453.1?		
	T	C5n.1n	9.592		453.5?		
	B	C5n.1n	9.735		457.3?		
	T	C5n.2n	9.777		458.0–459.5?	458.0	
D19	FO	*Denticulopsis dimorpha*	9.8	50X-CC/51-2, 27	459.3/461.07		
R11	LO	*Cyrtocapsella japonica*	10.0	51X-5, 135–136/52X-5, 135–136	466.7/476.2		
	B	C5n.2n	10.834		498.0–507.0		
	T	C5r.2n	11.378		523.00		
D20	LCO	*Denticulopsis praedimorpha*	11.4	56X-2, 25/56X-4, 25	509.15/512.15		
	B	C5r.2n	11.434		526.00		
R12	LO	*Cyrtocapsella cornuta*	11.7	56X-5, 135–136/57X-5, 137–139	514.8/524.5		
R13	LO	*Lithopera renzae*	11.7	56X-5, 135–136/57X-5, 137–139	514.8/524.5		
	T	C5An.1n	11.852		520.70		
	B	C5An.1n	12.000		522.10		
	T	C5An.2n	12.108		523.00		
	B	C5An.2n	12.333		525.50		
D21	FO	*Simonseniella barboi*	12.4	57X-CC/58X-2, 25	526.7/528.45		
R14	FO	*Lychnocanoma nipponica magnacornuta*	12.5	57X-5, 137–139/58X-5, 135–136	524.5/534.1		
	T	C5Ar.1n	12.618		528.50		
	B	C5Ar.1n	12.649		530.00		

Table 4 (continued).

		Datum	Age (Ma)	Core, section, interval (cm) 145-884B-	Depth (mbsf)	Hole 884C depth (mbsf)	Hole 884E depth (mbsf)
	T	C5Ar.2n	12.718		531.00		
	B	C5Ar.2n	12.764		532.50		
D22	FO	*Denticulopsis praedimorpha*	12.8	58X-5, 25/58X-6, 25	532.75/534.25		
	T	C5AAn.1n	12.941		535.00		
D23	FCO	*Denticulopsis hustedtii*	13.1	58X-7, 25/58X-CC	535.75/536.4		
	B	C5ABn.1n #	13.476		542.30		
	T	C5Dn.1n #	14.164		550.00		
	T	C5Dn.1n #	14.608		559.00		
D24	FO	*Denticulopsis hustedtii*	14.2–14.6	60X-CC/61X-CC	555.6/565.3		
D25	FO	*Denticulopsis hyalina*	14.9–15.1	62X-4, 25/62X-6, 25	567.05/570.05		
R15	FO	*Dictyophimus splendens*	15.3	61X-5, 135–136/62X-5, 135–136	563/572.7		
R16	FO	*Eucyrtidium inflatum*	15.3	61X-5, 135–136/62X-5, 135–136	563/572.7		
R17	LO	*Corythospyris?* sp.	15.3	61X-5, 135–136/62X-5, 135–136	563/572.7		
R18	FO	*Eucyrtidium asanoi*	15.8	62X-5, 135–136/63X-5, 135–136	572.7/582.2		
	T	C5Cn.1n? #	16.035		580		
D26	FO	*Denticulopsis lauta*	15.9	63X-3, 25/63X-4, 25	578.05/579.55		
D27	FO	*Denticulopsis praelauta*	16.2	63X-CC/64X-1, 25	584.4/584.65		
R19	FO	*Theocorys redondoensis*	16.25	63X-5, 135–136/64X-4, 135–136	582.2/590.3		
R20	FO	*Corythospyris?* sp.	16.7	63X-5, 135–136/64X-4, 135–136	582.2/590.3		
R21	LO	*Cenosphaera* sp.	16.7	63X-5, 135–136/64X-4, 135–136	582.2/590.3		
D28	FO	*Crucidenticula kanayae*	16.9	64X-4, 28/64X-5, 25	589.15/590.65		
	T	C5Dn.1n? #	17.31		594.2		
	B	C5Dn.1n? #	17.65		599		
	T	C5En.1n? #	18.317		602.8		
R22	FO	*Cycladophora cosma cosma*	17.25	64X-4, 135-135/65X-5, 135–136	590.3/601.5		
D29	FO	*Crucidenticula sawamurae*	18.4	65X-CC/66X-1, 25–26	603.8/604.05		
	B	C6n.1n? #	20.162		610		
D30	FO	*Thalassiosira fraga*	20.1	66X-5, 25–26/66X-5, 25–26	610.05/611.55		
D31	LO	*Rocella gelida*	22.4	67X-3, 25–26/67X-4, 25–26	616.54/618.04		
R23	FO	*Cryptocapsella tetrapera*	22.6	65X-5, 135–136/66X-5, 134–135	601.45/611.14		
N1	LO	*Dictyococcites bisectus*	23.8	66X-CC/69X-5, 18–19	612.3/638.58		
D32	FO	*Thalassiosira praefraga*	24.0–24.3	67X-CC/68X-1, 25–26	622.8/623.05		
D33	FCO	*Rocella gelida*	26.2–26.4	69X-5, 25–26/69X-6, 25–26	638.65/640.15		
D34	FO	*Rocella vigilans*	30.2	71X-7, 25/71X-CC	660.95/661.3		
N2	LO	*Reticulofenestra umbilica*	31.7	70X-CC/71X-CC	651.7/661.3		
N3	LO	*Isthmolithus recurvus*	32.5	73X-4, 75–80/73X-5,140–145	676.25/678.40		
IS		Oxygen isotope increase	34.3	74X-7, 10–15/75X-3, 128–133	689.7/694.48		
N4	LO	*Discoaster saipanensis*	35.0	74X-1, 0–5/74X-7, 10–15	680.6/689.7		
N5	LO	*Discoaster barbadiensis*	35.0	79X-3, 114–119/79X-5, 113–118	732.94/734.43		
N6	FO	*Isthmolithus recurvus*	35.1	82X-3, 107–112/82X-4, 79–84	761.77/762.99		
N7	LO	*Chiasmolithus grandis*	37.1	83X-1, 72–77/83X-2, 26–31	768.12/769.16		
N8	LO	*Chiasmolithus solitus*	39.7	83X-1, 72–77/83X-2, 26–31	768.12/769.16		
P1	LO	*Acarinina bulbrooki*	40.5	82X-6, 60–63/86X-CC, 28–31	765.8/766.98		
N9	FO	*Discoaster bifax*	(43.7)	83X-3,10–15/83X-4, 51–56	770.5/772.41		
P2	FO	*Acarinina bulbrooki*	45.2	86X-3, 28–33/86X-4, 25–30	799.68/801.65		
N10	FO	*Nannotetrina fulgens*	47.0 (47.3)	86X-3, 20–25/86X-4, 20–25	799.6/801.6		
N11	LO	*Discoaster sublodoensis*	47.2	86X-5, 65–70 /87X-4, 93–98	803.05/811.53		
N12	FO	*Nannotetrina cristata*	47.8	Below 87X-6, 70–75	Below 814.3		

Note: Abbreviations and ages as in Tables 1 and 3. # = paleomagnetic boundaries identified by biostratigraphic correlation with Site 887.

Ólafsson, this volume; Basov, this volume). The age of the lowermost sediment interval recovered at Site 884 (Cores 145-884B-91X through 145-884B-88X) is uncertain, although the presence of a reworked specimen of *Discoaster mohleri* in Sample 145-884B-85X-CC suggests that upper Paleocene sediments may be either present at the site or located nearby (Shipboard Scientific Party, 1993d).

Unconformities

A possible unconformity in the middle part of the Oligocene may be present at about 661 mbsf in the lowermost part of Core 145-884B-71X based on the coincidence of the LO of the calcareous nannofossil *Reticulofenestra umbilica* (31.7 Ma) and the FO of the diatom *Rocella vigilans* (30.2 Ma; Table 4; Fig. 7). A sharp lithologic contact is present at the 24-cm interval of Section 145-884B-71X-7, separating brown claystone above from underlying white nannofossil chalk. Diatoms decline down section in abundance and preservation at this horizon (Gladenkov and Barron, this volume). Seismic reflection data reveal a reflector of moderate amplitude and continuity at this horizon (Hamilton, this volume), but major differences in physical properties are not apparent (Shipboard Scientific Party, 1993d). Unfortunately, the geochemical logging tool string did not penetrate to this depth because a bridge developed in Hole 884E at 654 mbsf. The magnetic susceptibility log, however, shows a peak between about 660 and 650 mbsf (Shipboard Scientific Party, 1993d), suggesting a disruption in the sedimentation style.

Benthic foraminifers suggest the possibility of an unconformity at the Eocene/Oligocene boundary (Pak and Miller, this volume) or at about 695 mbsf, coinciding with the break between lithologic Subunits IIA and IIB (Shipboard Scientific Party, 1993d). Although these lithologic units are both claystone mixed with nannofossil chalk, evidence for soft-sediment deformation and large-scale redeposition is common in Subunit IIB, while such evidence is much less commonplace in Subunit IIA (Shipboard Scientific Party, 1993d). Although no hiatus is apparent in the age vs. depth plot (Fig. 7), an abrupt upsection decrease in the sediment accumulation rate from 70 m/m.y. to 12 m/m.y. is present at the Eocene/Oligocene boundary that may mark the onset of the Meiji drift sediments (Rea et al., this volume).

A third possible unconformity at about 769 mbsf in the middle part of Core 884B-83X separates middle Eocene sediments from upper Eocene sediments (ca. 42–35.5 Ma; Fig. 7). It is marked by the boundary between lithologic Subunit IIC, claystone, altered clayey ash, and ash, and overlying Subunit IIB, which is made up of chalk, claystone, and minor ash (Shipboard Scientific Party, 1993d). Soft-sediment deformation and evidence of large-scale redeposition, which typifies Subunit IIB, decreases abruptly down section in Subunit IIC, suggesting a change in the style of sedimentation (Shipboard Scientific Party, 1993d). At the depth of this contact, seismic reflection data reveal a reflector that separates a unit of flat-lying reflectors with moderate amplitudes from an overlying unit characterized by dipping, generally discontinuous reflectors with moderate to strong amplitudes (Hamilton, this volume). The age and duration of this un-

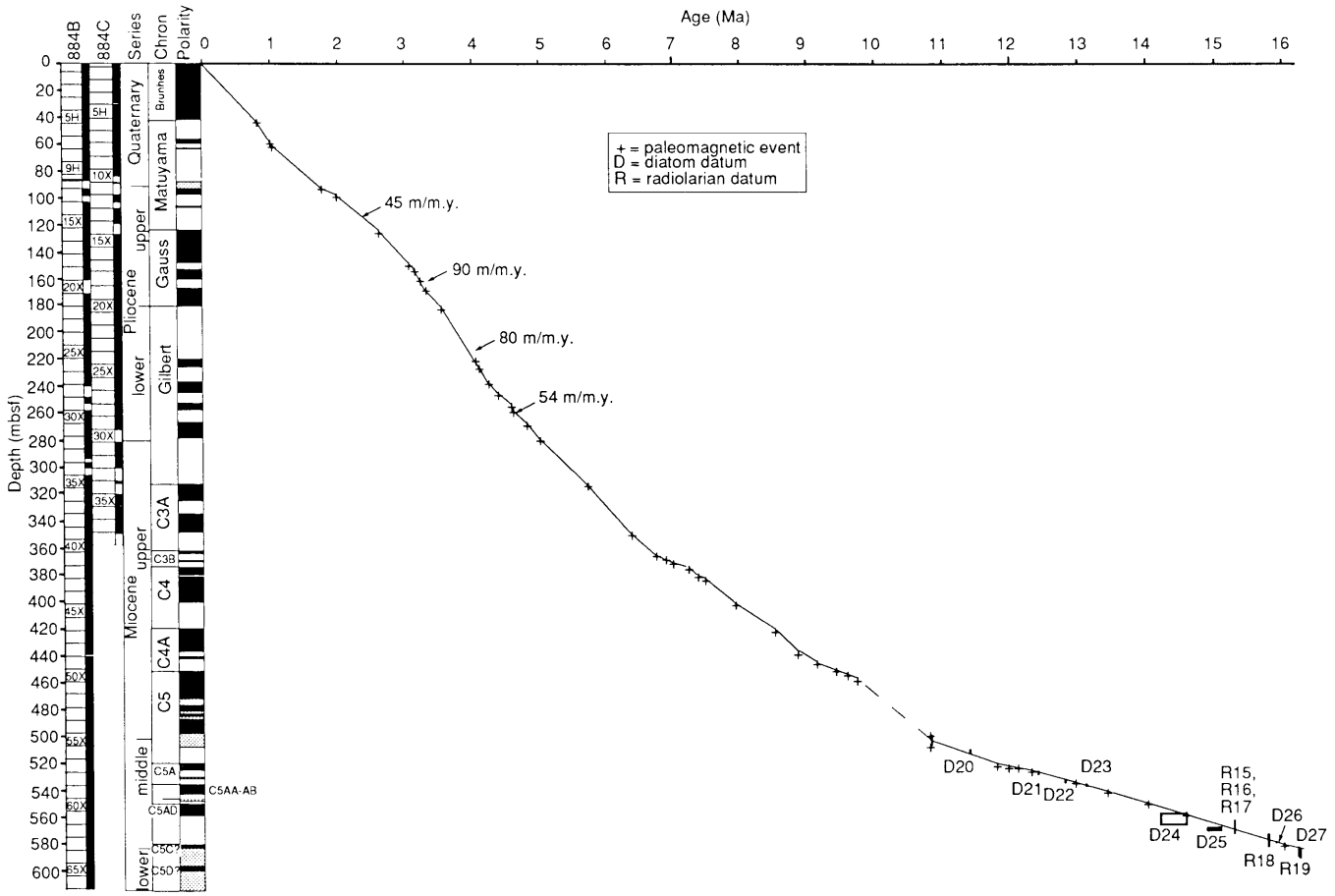

Figure 6. Age vs. depth plot of the middle Miocene through Quaternary section of Site 884 after Table 4.

conformity closely matches that of an unconformity at 710 mbsf in Hole 883B (42–34 Ma) and seems to indicate a major change in sedimentation style.

Site 887

Four holes were drilled at Site 887 (54°21.9′N, 148°26.8′W, 3645 m water) on the Patton-Murray Seamount in the northeast Pacific (Shipboard Scientific Party, 1993e). At Site 887, about 285 m of lower Miocene to Quaternary sediments overlie basalt encountered in Core 145-887D-4R. Below this interval a thin layer of sediment is found between basalt flows in Sample 145-887D-6R-1, 10–15 cm, which contains calcareous nannofossils indicative of an undifferentiated Oligocene age. Calcareous microfossils (foraminifers and calcareous nannofossils) range from barren to abundant and are moderately well to poorly preserved. The low diversity of the calcareous microfossil assemblages prevents the assignment of biostratigraphic zones to the samples. Siliceous microfossils (diatoms, radiolarians, and silicoflagellates), on the other hand, are more common in the sediments from Site 887 and are typically well preserved to moderately well preserved, but persistent reworking of middle Miocene diatoms and radiolarians is present in the uppermost Miocene and Pliocene part of the section.

High-quality paleomagnetic stratigraphy at Site 887 extends without interruption back to magnetic-polarity Subchron C5En (Table 5, Fig. 8), and the identification of the various paleomagnetic chrons is in good agreement between the biostratigraphers (Barron and Gladenkov, this volume; Morley and Nigrini, this volume) and the independent suggestions of the paleomagneticists (Weeks et al., this volume). The interval and subbottom depths of magnetostratigraphic polarity boundaries and biostratigraphic events are listed for Holes 887A and 887C in Table 5. An age vs. depth curve for Site 887 is constructed in Figure 8, mainly from magnetostratigraphy.

Unconformity

The middle Miocene *Crucidenticula nicobarica* Zone may be missing at an unconformity near 245 mbsf in Hole 887A. Sample 145-887A-27H-3, 20 cm (244.4 mbsf) is assignable to the *D. praedimorpha* Zone (11.4–12.8 Ma), whereas Sample 145-887A-27H-3, 124 cm (245.44 mbsf) belongs to the *Denticulopsis hyalina* Zone (13.1–15.1 Ma). No lithologic evidence, however, is apparent for an unconformity in this interval (Shipboard Scientific Party, 1993e). If present, such a hiatus would coincide with the early part of a major hiatus at Site 883 (Fig. 4).

CONCLUSIONS

Biochronology

The Pliocene and Pleistocene magnetostratigraphic records of Sites 881–884 and 887 (Figs. 2–4, 6, 8) provide a framework for evaluation of the isochroneity and diachroneity of microfossil events. As many as eleven diatom, seven radiolarian, and five calcareous nanno-

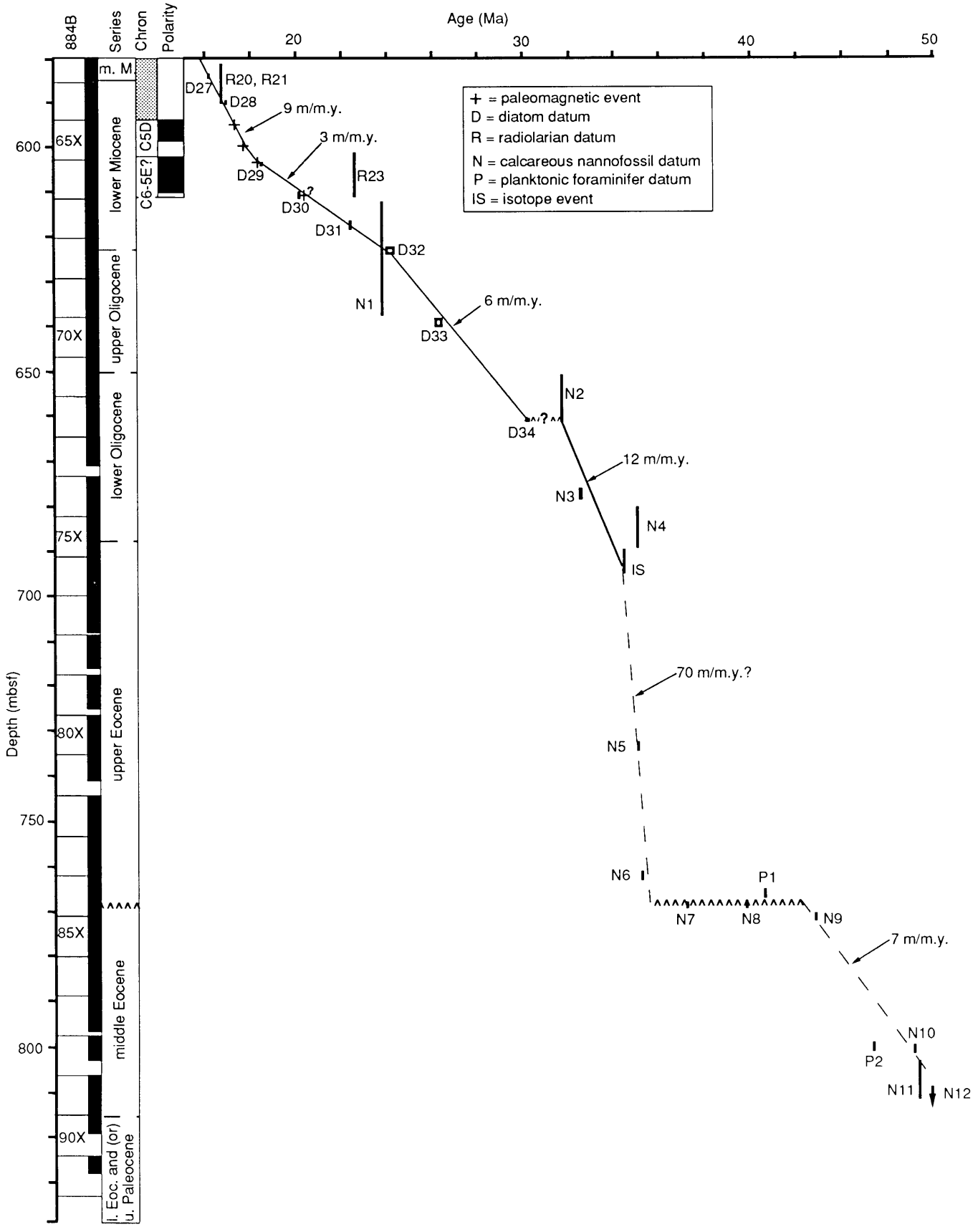

Figure 7. Age vs. depth plot of the middle Eocene through lower Miocene section of Site 884 after Table 4.

Table 5. Age, interval, and depth of magnetostratigraphic polarity boundaries and biostratigraphic datum levels in Holes 887A and 887C.

		Datum	Age (Ma)	Core, section, interval (cm) 145-887A-	Depth (mbsf)	Core, section, interval (cm) 145-887C-	Depth (mbsf)
R1	LO	*Lychnocanoma nipponica sakaii*	0.05	1H-1, 12–13/1H-3, 52–53	0.12/3.52		
N1	FO	*Emiliania huxleyi*	0.294	1H-3, 110–111/1H-4, 110–111	4.10/5.60		
D1	LO	*Simonseniella curvirostris*	0.3	2H-CC/3H-CC	16.2/25.7		
R2	LO	*Stylacontarium acquilonium*	0.4	3H-3, 132–133/4H-1, 12–13	20.52/25.82		
R3	LO	*Stylatractus universus*	0.55	4H-1, 12–13/4H-3, 132–133	25.82/30.02		
	B	C1n.1n	0.78		45.55		42.7
	T	C1r.1n	0.984		55.6		52.6
R4	LO	*Eucyrtidium matuyamai*	1.0	7H-3, 54–55/7H-6, 54–55	57.74/62.24		
D2	LCO	*Actinocyclus oculatus*	1.0	6H-CC/7H-CC	54.2/63.7		
	B	C1r.1n	1.049		58.95		56.25
D3	FO	*Simonseniella curvirostris*	1.58	7H-CC/8H-CC	63.7/73.2		
N2	FO	*Gephyrocapsa oceanica*	1.674	5H-2, 110–111/5H-6, 110–111	37.80/43.80		
R5	LO	*Sphaeropyle robusta*	1.5–1.7	8H-3, 54–55/8H-6, 54–55	67.24/71.74		
	T	C2n.1n	1.757				75.35
	B	C2n.1n	1.983				78.95
D4	LO	*Neodenticula koizumii*	2.0	8H-CC/9H-CC	73.2/82.7		
	FO	*Eucyrtidium matuyamai*	2.0	9H-3, 54–55/10H-3, 54–55	76.74/86.24		
	T	C2An.1n	2.60		88.9		87.3
D5	LCO	*Neodenticula kamtschatica*	2.63–2.7	9H-CC/10H-CC	82.7/92.2		
D6	FO	*Neodenticula seminae*	2.7	9H-CC/10H-CC	82.7/92.2		
R6	FO	*Cycladophora davisiana davisiana*	2.9	11H-3, 54–55/12H-3, 54–55	95.74/105.24		
	B	C2An.1n	3.054		101.1		98.3
	T	C2An.2n	3.127		101.85		100.55
	B	C2An.2n	3.221		104.2		102.7
D7	LO	*Thalassiosira marujamica*	3.1–3.2	12H-2, 135/12H-3, 5	104.55/104.75		
	T	C2An.3n	3.325		106.55		103.4
	B	C2An.3n	3.553		110.35		105.9
D8	FO	*Actinocyclus oculatus*	3.65–3.85	13H-1, 21/13H-2, 21	111.4/112.9		
D9	FO	*Neodenticula koizumii*	3.51–3.85	13H-2, 21/13H-3, 21	112.9/114.4		
	T	C3n.1n	4.033		121.1		120.35
	B	C3n.1n	4.134		125.2		
	B	C3n.2n	4.432		134.7		134.8
	T	C3n.3n	4.611				139.65
	B	C3n.3n	4.694		142.2		
D10	LO	*Thalassiosira jacksonii* (plicate)	4.5–4.6	16X-CC/17X-1, 21	144.37/145.3		
	T	C3n.4n	4.812		145.8		143.55
D11	FO	*Thalassiosira latimarginata*	4.8–4.9	17X-3, 21/17X-4, 21	148.3/149.8		
	B	C3n.4n	5.046		149.95		148.65
D12	FO	*Thalassiosira oestrupii*	5.3	17X-CC/18H-1, 21	154.8/155.0		
	T	C3An.1n	5.705				169–169.3
	B	C3An.1n	5.946				177.1
	T	C3An.2n	6.078				181.75
D13	FO	*Thalassiosira miocenica*	6.2	21X-1, 22/21X-2, 22	183.9/185.4		
	B	C4n.1n	7.376				199.2
D14	FO	*Neodenticula kamtschatica*	7.1–7.2	22H-4, 21/22H-5, 21	198.1/199.6		
D15	FO	*Nitzschia reinholdii*	7.2–7.3	22H-5, 21/22H-6, 21	199.6/201.1		
D16	LCO	*Thalassionema schraderi*	7.4	22H-6, 21/22H-CC	201.1/202.9		
	T	C4n.2n	7.464				199.8
R7	FO	*S. delmontensis* > *S. peregrina*	7.55	22H-6, 54–55/23H-6, 54–55	201.44/210.94		
R8	LO	*Prunopyle hayesi*	7.6	22H-6, 54–55/23H-6, 54–55	201.44/210.94		
R9	FO	*Stylacontarium acquilonium*	7.7	22H-6, 54–55/23H-6, 54–55	201.44/210.94		
	B	C4n.2n	7.892				205.45
	T	C4r.1n	8.047				206.8
D17	LCO	*Denticulopsis hustedtii*	8.4	23H-7, 21/23H-CC	212.1/212.4		
	T	C4r.2r-1	8.463				211.25
	B	C4r.2r-1	8.479				211.65
	T	C4An.1n	8.529				211.8
R10	LO	*Lychnocanoma nipponica magnacornuta*	8.8	23H-6, 54–55/24H-3, 54–55	210.94/215.94		
	B	C4An.1n	8.861				215.95
D18	LO	*Denticulopsis dimorpha*	9.0	24H-4, 21/24H-5, 21	217.1/218.6		
	T	C4r.2n	9.428				219.75
	B	C4Ar.2n	9.491				220.65
	T	C5n.1n	9.592				221.3
	B	C5n.1n	9.735				222.85
	T	C5n.2n	9.777				223.05
D19	FO	*Denticulopsis dimorpha*	9.8	25H-3, 133/25H-4, 133	226.23/227.73		
R11	LO	*Cyrtocapsella japonica*	10.0	24H-6, 54–55/25H-3, 54–55	220.44/225.44		
	B	C5n.2n	10.834				231.45
	T	C5r.2n	11.378				235.15
D20	LCO	*Denticulopsis praedimorpha*	11.4	25H-CC/27H-1, 60	231.4/241.82	6H-6, 21 /26H-7, 21	234.0/235.5
R12	LO	*Cyrtocapsella cornuta*	11.7	26H-6, 55- 56/27H-3, 55–56	234.35/239.35		
	T	C5An.1n	11.852				238.25
	B	C5An.1n	12.00				239.5
	T	C5An.2n	12.108				240.05
	B	C5An.2n	12.333				241.65
D21	FO	*Simonseniella barboi*	12.4	25H-CC/27H-1, 60	231.4/241.82	7H-3, 21/27H-6, 21	239.0/243.5
R13	FO	*Lychnocanoma nipponica magnacornuta*	12.5			27H-3, 55–56/27H-6, 55–56	239.35/243.85
	T	C5Ar.1n	12.618				243.05
	B	C5Ar.1n	12.649				243.25
	T	C5Ar.2n	12.718				243.45
	B	C5Ar.2n	12.764				243.75
D22	FO	*Denticulopsis praedimorpha*	12.8	27H-3, 20/27H-3, 124	244.4/245.44	27H-6, 21/27H-CC	243.5./245.3
D23	FCO	*Denticulopsis hustedtii*	13.1	27H-3, 20/27H-3, 124	244.4/245.442	7H-6, 21/27H-CC	24.5./245.3
	B	C5ABn	13.476				247.25
	T	C5ACn.1n	13.674				248.45
	B	C5ACn.1n	14.059				250.85

Table 5 (continued).

		Datum	Age (Ma)	Core, section, interval (cm) 145-887A-	Depth (mbsf)	Core, section, interval (cm) 145-887C-	Depth (mbsf)
	T	C5ADn.1n	14.164				251.75
	T	C5Bn.1n	14.8				255.6
	B	C5Bn.1n	14.89				256.25
D24	FO	*Denticulopsis hyalina*	14.9	29H-1, 51/29H-2, 21	260.7/261.9		
	T	C5Bn.2n	15.038				257.05
	B	C5Bn.2n	15.162				257.55
R14	FO	*Dictyophimus splendens*	15.3	28H-6, 55–56/29H-3, 54–55	258.75/263.74		
R15	FO	*Eucyrtidium inflatum*	15.3	28H-6, 55–56/29H-3, 54–55	258.75/263.74		
R16	LO	*Corythospyris?* sp.	15.3	28H-6, 55–56/29H-3, 54–55	258.75/263.74		
R17	FO	*Eucyrtidium asanoi*	15.8	28H-6, 55–56/29H-3, 54–55	258.75/263.74		
	T	C5Cn.1n	16.035				262.1
R18	FO	*Theocorys redondoensis*	16.25	28H-6, 55–56/29H-3 54–55	258.75/263.74		
R19	FO	*Corythospyris?* sp.	16.7	Below 29H-3, 54–55	Below 263.74	Above 30H-3, 54–55	Above 267.84
R20	LO	*Cenosphaera* sp.	16.7	Below 29H-3, 54–55	Below 263.74	Above 30H-3, 54–55	Above 267.84
D25	FO	*Crucidenticula kanayae*	16.9	Below 29H-3, 54–55	Below 263.74	30H-1, 21 /30H-2, 21	264.51/266.01
R21	FO	*Cycladophora cosma cosma*	17.25	Below 29H-3, 54–55	Below 263.74	Above 30H-3, 54–55	Above 267.84
	T	C5Dn.1n	17.31				266.75
	B	C5Dn.1n	17.65				268.4
	T	C5En.1n	18.317				271.95
D26	FO	*Crucidenticula sawamurae*	18.4	Below 30X-CC	Below 279.4	30H-6, 21/30H-7, 21	272.0/273.7
D27	FO	*Thalassiosira fraga*	20.1			Below 30H-CC	Below 273.8

Note: Abbreviations as in Tables 1 and 3.

fossil events appear to be isochronous for correlation of Pliocene and Pleistocene sediments across the middle to high latitudes in the North Pacific (Tables 1–5). Calcareous nannofossils are useful for biostratigraphy only at the sites with shallower water depths (Site 882, 883, and 887), and they are very sparse within the thick diatomaceous sections that characterize the lower and lower upper Pliocene. Planktonic foraminiferal biostratigraphic studies on the Pliocene and Pleistocene sediments of Leg 145 are limited to a study of a very short interval of the middle part of the Pliocene of Sites 883 and 887 by Dowsett and Ishman (this volume).

A major contribution of Leg 145 is the recovery of the first continuous magnetostratigraphic records in the North Pacific for the upper lower Miocene through the upper Miocene (magnetic polarity Subchrons C5En through C3An) section at Sites 884 and 887 (Figs. 6, 8). These magnetostratigraphic records allow the first direct calibration of numerous diatom and radiolarian datum levels to magnetostratigraphy and establish the isochroneity (or diachroneity) of these microfossil events between the northwest and northeast Pacific (Barron and Gladenkov, this volume; Morley and Nigrini, this volume). Within the limits of available stratigraphy, at least fifteen diatom and fifteen radiolarian datum levels appear to be isochronous for Miocene correlations between Sites 884 and 887 (Tables 4, 5). Unfortunately, neither calcareous nannofossils nor planktonic foraminifers are present in sufficient numbers or diversity in the Miocene sections of Sites 884 and 887 to allow calibration to magnetic stratigraphy (Ólafsson and Beaufort, this volume; Shipboard Scientific Party, 1993d, 1993e).

Below the upper part of the lower Miocene section, microfossils provide the only means of assigning ages to the sediment record of Leg 145. Calcareous nannofossils are the most useful microfossil for correlations, with as many as 24 biostratigraphically important datum levels recognized in the Upper Cretaceous through upper lower Miocene section of Site 883 (Table 3; Ólafsson and Beaufort, this volume; Beaufort and Ólafsson, this volume). Planktonic foraminifers provide valuable correlations in the lower and middle Eocene sections, especially of Site 883 (Basov, this volume). Gladenkov and Barron (this volume) propose an Oligocene through lower Miocene diatom zonation based on their study of Site 884, whereas Shilov (this volume) documents the Eocene through early Miocene radiolarian assemblages at Sites 883 and 884 and suggests a preliminary zonation.

The Sediment Record

Although the age vs. depth plots reveal that the Pliocene and Pleistocene record is complete at Sites 881–884 and 887 (Figs. 2–4, 6, 8), sediment accumulation rates vary considerably. Although thick sequences of diatomaceous sediment with sedimentation rates in excess of 100 m/m.y. characterize much of the Pliocene (ca. 4.4 to 2.6 Ma) of Sites 882 and 883 (Figs. 3, 4), this same interval is marked by rates (ca. 33 m/m.y.) that are reduced compared to those of the post-2.6-Ma Pliocene and Pleistocene record at Site 881 (Fig. 2). These differences clearly reflect both the better preservation of carbonate and smaller, more finely silicified diatom taxa at Sites 882 and 883 on the top of Detroit Seamount (Haug et al., this volume) and an increase in the amount of abyssal transport in the younger record of deeper Site 881 (Rea et al., this volume).

The upper Miocene section is generally complete at Sites 883, 884, and 887, but two unconformities, (ca. 7.7–7.1 Ma) and (6.1–5.3 Ma), appear to be present at Site 881. The older of these two hiatuses appears to correlate with hiatus NH6 of Keller and Barron (1987) (7.7–6.5 Ma updated age), which is widespread in the North Pacific and appears to reflect an event of intensification of bottom currents. The younger hiatus, on the other hand, is slightly older than hiatus NH7 of Keller and Barron (1987), which has an updated age of 5.5 to 5.0 Ma.

With the exception of a compressed interval of the *Denticulopsis praedimorpha* diatom Zone (12.8–11.4 Ma), the lowermost part of the upper Miocene section and the entire upper middle Miocene section (14.2–10.2 Ma) is removed at one or more unconformities between about 556 and 547 mbsf at Site 883. At Site 884 on the east flank of Detroit Seamount, this 14.2–10.2-Ma interval is largely represented by lithologic Subunit IC, a dark-gray to gray claystone, which contains reduced numbers of diatoms and radiolarians (>20% opal) (Shipboard Scientific Party, 1993d). A series of high-frequency discontinuous seismic reflectors in this interval of Site 884 (Hamilton, this volume) may be suggestive of the intensification of bottom currents. At Site 887 in the northwest Pacific, this late middle Miocene unconformity, if present, is restricted to the *Crucidenticula nicobarica* diatom Zone or from about 13.1–12.8 Ma (Fig. 8). Keller and Barron (1987) note the widespread occurrence of hiatuses NH3 and NH4 in the North Pacific, which correspond, respectively, with the intervals ranging from 13.0 to 12.1 Ma and 10.9–10.1 Ma.

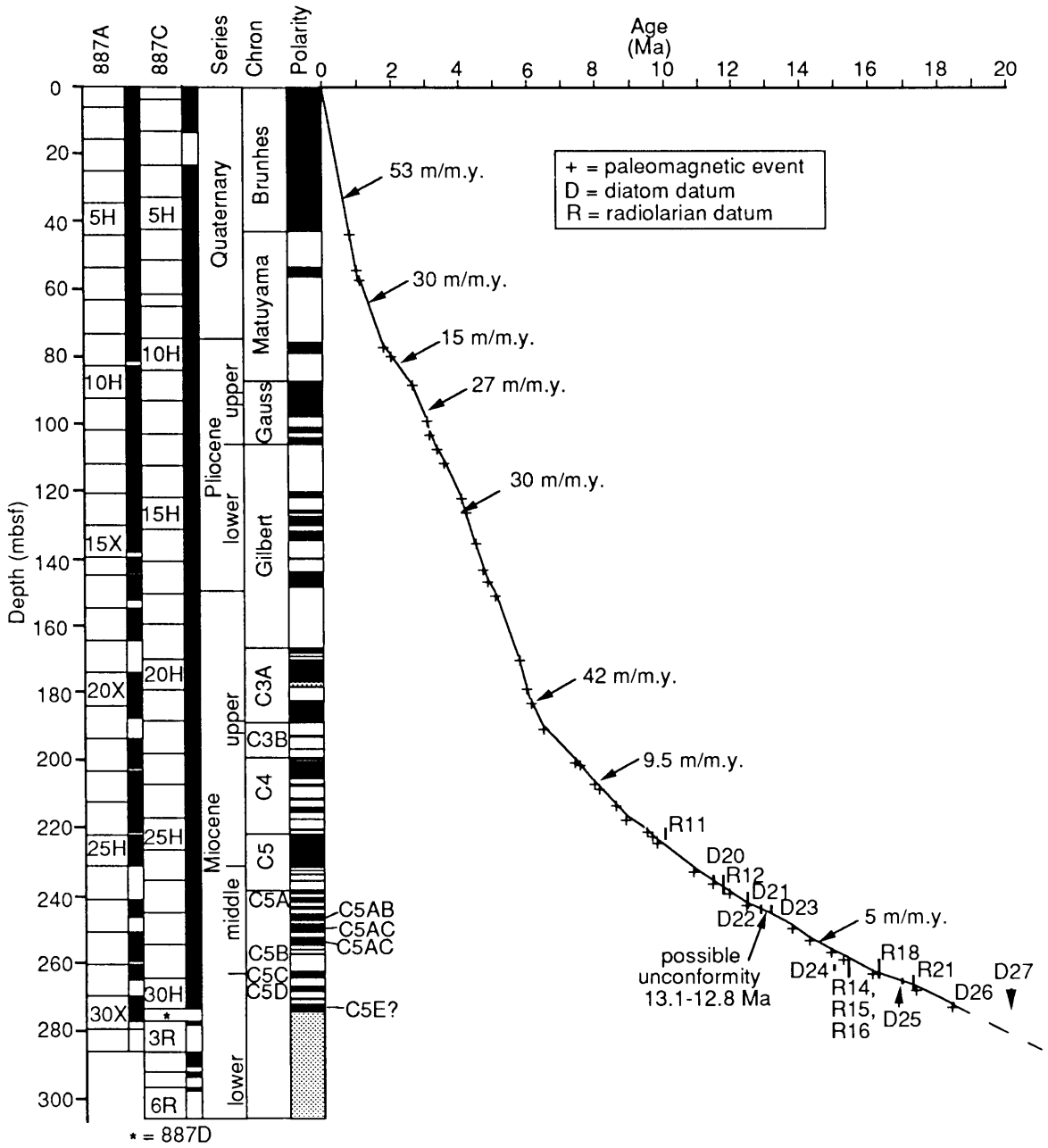

Figure 8. Age vs. depth plot of Site 887 after Table 5.

Extensive records of the Paleogene and lower Miocene are restricted to Sites 883 and 884. Whereas Site 884 appears to have the more complete upper Eocene through lower Miocene record of the two sites (Fig. 7), the lower Eocene through middle Eocene record appears to be more complete at Site 883 (Fig. 5), which also is characterized by better carbonate preservation. In addition, much of the Eocene record of Site 884 is chaotic and apparently redeposited (Shipboard Scientific Party, 1993d; Beaufort and Ólafsson, this volume). Both Sites 883 and 884 contain major unconformities at the middle Eocene/upper Eocene boundary, which appear to commence at about 42 Ma, the age of the major change in the motion of the Pacific plate that is associated with the bend in the Emperor Seamount Chain. This major hiatus continues to about 34 Ma (latest Eocene) in age at Site 883 (Fig. 5), but apparently ceases slightly earlier (at ca. 35.5 Ma; late Eocene) at Site 884.

Paleocene sediments are limited to a thin section in the lower part of Core 145-883B-85X and the upper part of Core 145-883E-19R (Beaufort and Ólafsson, this volume; Pak and Miller, this volume) where a compressed section of upper Paleocene sediments unconformably overlies a thin sequence of nannofossil-bearing ashes of Late Cretaceous age at the base of the Site 883 sediment section. Calcareous nannofossils in Cores 145-883B-86X and 145-883B-87X appear to be Maestrichtian in age (Beaufort and Ólafsson, this volume).

ACKNOWLEDGMENTS

This manuscript benefited from the reviews of Bill Sliter, Kris McDougall, Tim Bralower, and David Harwood and we are grateful for their suggestions. The research of various scientists was funded

by the various programs and grants listed in the acknowledgments of their individual chapters. We are grateful to David Rea and the other scientists and crew members of Leg 145 of the *JOIDES Resolution* for their support and encouragement.

REFERENCES*

Aubry, M.-P., Berggren, W.A., Kent, D.V., Flynn, J.J., Klitgord, K.D., Obradovich, J.D., and Prothero, D.R., 1988. Paleogene geochronology: an integrated approach. *Paleoceanography*, 3:707–742.

Barron, J.A., 1989. The late Cenozoic stratigraphic record and hiatuses of the northeast Pacific: results from the Deep Sea Drilling Project. *In* Winterer, E.L., Hussong, D.M., and Decker, R.W. (Eds.), *The Geology of North America* (Vol. N): *The Eastern Pacific Ocean and Hawaii*. Geol. Soc. Am., Geol. of North America Ser., 311–322.

Berggren, W.A., Kent, D.V., and Flynn, J.J., 1985a. Jurassic to Paleogene, Part 2. Paleogene geochronology and chronostratigraphy. *In* Snelling, N.J. (Ed.), *The Chronology of the Geological Record*. Geol. Soc. London Mem., 10:141–195.

Berggren, W.A., Kent, D.V., and Van Couvering, J.A., 1985b. The Neogene, Part 2. Neogene geochronology and chronostratigraphy. *In* Snelling, N.J. (Ed.), *The Chronology of the Geological Record*. Geol. Soc. London Mem., 10:211–260.

Cande, S.C., and Kent, D.V., 1992. A new geomagnetic polarity time scale for the Late Cretaceous and Cenozoic. *J. Geophys. Res.*, 97:13917–13951.

Keller, G., and Barron, J.A., 1987. Paleodepth distribution of Neogene deep-sea hiatuses. *Paleoceanography*, 2:697–713.

Leroux, S., 1993. Susceptibilité magnétique de sédiments: comparaison entre les diagraphies et les mesures sur carotte-intérêt. Magnétostratigraphie sur carottes de forages (ODP Leg 145, Puits 883B). *Mém. DEA, Ecole Normale Supérieure.*

Rea, D.K., Basov, I.A., Janecek, T.R., Palmer-Julson, A., et al., 1993. *Proc. ODP, Init. Repts.*, 145: College Station, TX (Ocean Drilling Program).

Shipboard Scientific Party, 1993a. Site 881. *In* Rea, D.K., Basov, I.A., Janecek, T.R., Palmer-Julson, A., et al., *Proc. ODP, Init. Repts.*, 145: College Station, TX (Ocean Drilling Program), 37–83.

———, 1993b. Site 882. *In* Rea, D.K., Basov, I.A., Janecek, T.R., Palmer-Julson, A., et al., *Proc. ODP, Init. Repts.*, 145: College Station, TX (Ocean Drilling Program), 85–119.

———, 1993c. Site 883. *In* Rea, D.K., Basov, I.A., Janecek, T.R., Palmer-Julson, A., et al., *Proc. ODP, Init. Repts.*, 145: College Station, TX (Ocean Drilling Program), 121–208.

———, 1993d. Site 884. *In* Rea, D.K., Basov, I.A., Janecek, T.R., Palmer-Julson, A., et al., *Proc. ODP, Init. Repts.*, 145: College Station, TX (Ocean Drilling Program), 209–302.

———, 1993e. Site 887. *In* Rea, D.K., Basov, I.A., Janecek, T.R., Palmer-Julson, A., et al., *Proc. ODP, Init. Repts.*, 145: College Station, TX (Ocean Drilling Program), 335–391.

Wei, W., and Peleo-Alampay, A., 1993. Updated Cenozoic nannofossil magnetobiochronology. *INA Newsl.*, 15:15–21.

Zijderveld, J.D.A., Zachariasse, W.J., Verhallen, P.J.J.M., and Hilgen, F.J., 1986. The age of the Miocene-Pliocene boundary. *Newsl. Stratigr.*, 16:169–181.

*Abbreviations for names of organizations and publications in ODP reference lists follow the style given in *Chemical Abstracts Service Source Index* (published by American Chemical Society).

Date of initial receipt: 29 September 1994
Date of acceptance: 23 January 1995
Ms 145SR-145